

pubs.acs.org/acscatalysis Review

# **Encapsulation Methods for Control of Catalyst Deactivation: A Review**

Hope O. Otor, Joshua B. Steiner, Cristina García-Sancho,\* and Ana C. Alba-Rubio\*



Cite This: ACS Catal. 2020, 10, 7630-7656



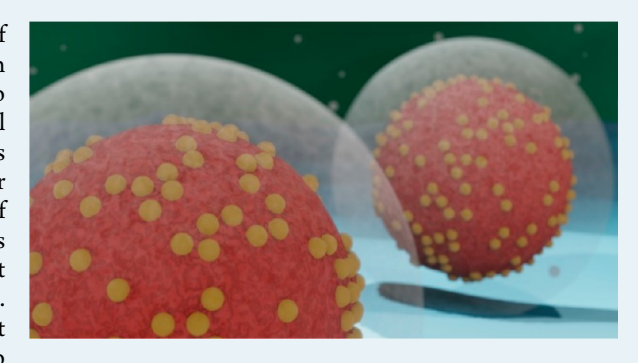
**Read Online** 

**ACCESS** 

Metrics & More

Article Recommendations

ABSTRACT: One of the most significant challenges in the use of heterogeneous catalysts is the loss of activity and/or selectivity with time on stream, and researchers have explored different methods to overcome this problem. Recently, the coating of catalysts to control their deactivation has generated much research traction. This Review is aimed at studying different encapsulation techniques employed for controlling catalyst deactivation. Focus is given to the prevention of irreversible modes of deactivation, such as sintering and leaching. In this Review, we elaborate on different entrapment methods used to protect catalysts from deactivation in both liquid and gas reaction media. Relevant probe reactions are discussed with emphasis on the catalyst activity and stability. Challenges associated with those processes are also



described with emphasis on the mass transfer limitations as a result of the coverage of the active sites. Finally, some future perspectives and areas for possible improvement are highlighted.

KEYWORDS: catalyst deactivation, encapsulation, stability, leaching, sintering, ALD, SMSI, core-shell

### 1. INTRODUCTION

Catalyst deactivation, which is the loss of catalyst activity and/ or selectivity with time on stream, is a major drawback in the industrial applications of heterogeneous catalysts, as a considerable amount of time and resources are invested on catalyst replacement or regeneration, when possible. Different modes of deactivation associated with catalytic systems include leaching, sintering, coking, phase transition, poisoning, fouling, and attrition/crushing. These deactivation modes are further classified as chemical, mechanical, or thermal. The ubiquitous nature of heterogeneous catalysis, the invaluable role that they play in many reaction systems, and the painstaking efforts involved in designing these catalytic structures make it imperative to ensure their long-term stability.

While processes like sintering and leaching lead to irreversible deactivation on catalysts, other mechanisms like coking can be reversed by subjecting the catalyst to a calcination step in the presence of air or oxygen to burn the carbonaceous species deposited onto the catalyst surface. As such, many efforts are targeted toward preventing irreversible deactivation mechanisms. Sintering is the agglomeration of supported active materials (active sites and/or support) via particle migration and coalescence, or Ostwald ripening, <sup>2,6</sup> and leaching is the dissolution of the active sites into the reaction medium. <sup>7</sup> Whereas sintering is more prevalent in gas-phase reactions, leaching dominates in liquid media. The likelihood

of sintering occurring in liquid media depends on the reaction conditions and the tendency of the metallic particles to migrate and coalesce, forming bigger particles. Leaching also poses significant challenges besides the obvious loss of active sites and reactivity, as it also incurs a downstream separation step to obtain the purified reaction product.

Some other deactivation modes can be easily prevented by feed purification, which is typical in scenarios where the catalyst poisoning is prevalent, as in the case of systems containing sulfur-rich feeds. Other strategies, such as the reactor design and modification of the shape and structure of the catalysts have also been utilized to minimize mechanical modes of deactivation like attrition; however, care must be taken to maintain a good surface-area-to-volume ratio to ensure that the active sites are exposed to the reacting species. Modifications of the feed composition and reaction conditions, such as temperature and pressure, have also been explored as approaches to mitigate the catalyst deactivation. Nevertheless, there is a limit to which these conditions can be altered without having a negative effect on the catalytic activity.

Received: April 6, 2020 Revised: May 27, 2020 Published: June 2, 2020



Recently, greater research focus has been geared toward the encapsulation of heterogeneous catalysts to prevent their deactivation. Different mechanisms, such as atomic layer deposition (ALD), strong metal-support interaction (SMSI), nonhydrolytic sol-gel, and core-shell methods have been successfully used to coat the catalysts with marked improvement on their stability. Some earlier reviews have discussed different strategies for control of catalyst deactivation. For example, Lange et al. reported the challenges associated with the use of renewable feedstocks (fouling and poisoning) and discussed relevant mitigation approaches. Héroguel et al. also discussed different combative strategies to prevent catalyst deactivation in liquid-phase biomass conversion and reforming. 10 Recently, Goodman et al. reported the mechanisms of sintering and the characterization techniques used to distinguish them, and they also provided insights on the rational design of sinter-resistant catalysts.<sup>2</sup> While most reviews have focused on a single deposition technique (e.g., ALD<sup>11</sup> or SMSI<sup>12</sup>), this report compares several strategies coming from different fields that are rarely compared. Here we provide a global perspective on the advances of encapsulation technologies for control of catalyst deactivation. Major emphasis is on the encapsulation of base and noble metals against deactivation in both gas and liquid reaction media, with particular attention given to the impacts of these techniques in improving the stability and activity of the coated catalyst and the associated mass transfer limitations. Relevant probe reactions, such as CO oxidation, syngas methanation, methane-based reactions, and aqueous-phase hydrogenation mostly used for biomass conversion, have been used to elucidate the effectiveness of these methods.

# 2. CHEMICAL VAPOR DEPOSITION (CVD)

Chemical vapor deposition (CVD), which is a technique employed in coating, is induced by a chemical reaction between a carrier gas and a vapor phase at the surface of a substrate. Typically, substrates for CVD reaction are usually heated to elevated temperatures before the CVD process, and the precursor substances decompose on the surface thereby growing into a thin film. CVD finds significant application in the deposition of graphene on copper, synthesis of carbon nanotubes (CNTs), sapplication in photovoltaic cells, and growing of 2D materials for utilization in electronics and semiconductor design. Parameters such as the substrate type, choice of precursor, pressure, and temperature of the system, affect the general mechanism of CVD growth and the associated heat and mass transfer phenomena, and thus, proper attention is given in selecting these parameters.

Seipenbusch and Binder published an early report stabilizing catalysts using CVD. <sup>20</sup> They made use of a thin silica coating deposited by CVD to stabilize palladium nanoparticles from loss of surface area during tempering using two different approaches: coating of nonagglomerated particles and coating of agglomerated particles. In the first instance, spherical metal particles generated with a spark discharge generator (SDG) were exposed to a nitrogen flow doped with the silica precursor (tetraethylorthosilicate (TEOS)) before entering a furnace at 800 °C. In this furnace, the adsorbed precursor decomposed depositing silica on the particle surface, after which the aerosol was given enough time to agglomerate in another tube. However, in the second approach, the particles were first allowed to agglomerate in a tube before being subjected to the silica precursor stream for coating and sintering tests. In both

methods, the mobility of the primary particles was monitored using electrical mobility analysis, while the sintering of particles was investigated using transmission electron microscopy (TEM). Based on the sintering kinetic experiments performed and the size distribution obtained from the TEM analysis, it was observed that the primary particles were stabilized from coalescence when using the first approach, but their rearrangement could not be inhibited. The rearrangement of the primary particles was only inhibited in the second case, in which the structure was coated as a whole. Using the hydrogenation of ethene as a probe reaction, the stabilized catalyst experienced a reduction in the catalytic activity of about 23%. This would appear as an acceptable trade-off when compared with an uncoated catalyst that would significantly reduce its activity at high temperatures because of sintering.

Although CVD has been less frequently used for stabilizing catalysts because of the formation of thick, nonuniform overcoats, Xiong et al. used CVD of graphitic carbon to stabilize an alumina support  $(gc-Al_2O_3)$ . Figure 1 shows the

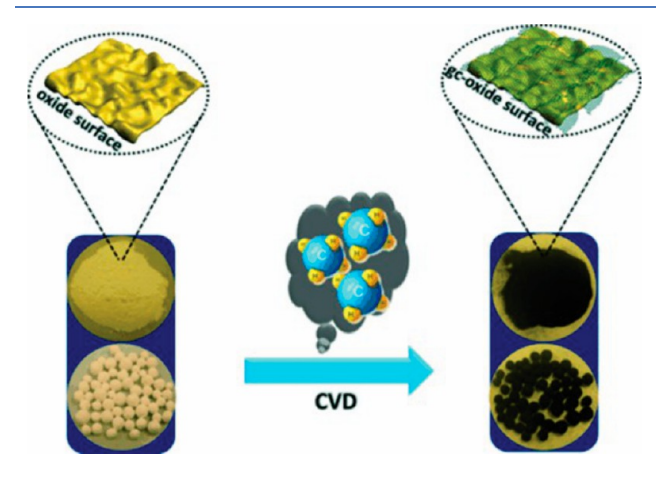


**Figure 1.** Schematic describing the preparation of gc-Al $_2$ O $_3$  by CVD. Performing the premission from ref 21. Copyright 2015 John Wiley and Sons.

preparation scheme, in which methane was used as the carbon source with exposure times varying from 0.5 to 6 h at 900  $^{\circ}\text{C}$ . The hydrothermal stability of alumina and the gc-Al<sub>2</sub>O<sub>3</sub> catalyst was studied in an autoclave reactor with water at 220  $^{\circ}\text{C}$  for 12 h. While the X-ray Diffraction (XRD) pattern for the gc-Al<sub>2</sub>O<sub>3</sub> catalyst showed little to no significant change upon the thermal treatment, the uncoated alumina sample exhibited peaks of boehmite (AlO(OH)) indicating a reaction between the alumina and water. The stability of the gc-Al<sub>2</sub>O<sub>3</sub> was markedly improved when the carbon loading was increased. This result indicated that the deposition of graphitic carbon improved the stability of the alumina in water at elevated temperatures. The stability of gc-coated alumina was attributed to the relative inertness of graphitic carbon, which acts as a physical barrier preventing the hydrolytic attack.

To further test the coated alumina in reactions, gc-Al<sub>2</sub>O<sub>3</sub> was used as a support to deposit Pt and Ru nanoparticles. Their catalytic behavior was investigated in two biomass-conversion model reactions: Pt/gc-Al<sub>2</sub>O<sub>3</sub> for the aqueous-phase reforming (APR) of ethylene glycol and Ru/gc-Al<sub>2</sub>O<sub>3</sub> for the aqueous-phase hydrogenation (APH) of lactic acid. While a Pt/ $\gamma$ -Al<sub>2</sub>O<sub>3</sub> catalyst showed deactivation through sintering and leaching because of the reaction of alumina with water, the Pt/gc-Al<sub>2</sub>O<sub>3</sub>

catalyst maintained its high activity with no apparent deactivation. A similar performance was observed with Ru/gc-Al<sub>2</sub>O<sub>3</sub> when compared with a Ru/ $\gamma$ -Al<sub>2</sub>O<sub>3</sub> catalyst. Whereas scanning transmission electron microscopy (STEM) images of the used Ru/ $\gamma$ -Al<sub>2</sub>O<sub>3</sub> catalyst showed the transformation of  $\gamma$ -Al<sub>2</sub>O<sub>3</sub> into boehmite with an associated increase in the Ru particle size, the Ru/gc-Al<sub>2</sub>O<sub>3</sub> catalyst remained unchanged.

Phaahlamohlaka et al. also used CVD to encapsulate Ru particles inside hollow carbon spheres (HCS).<sup>22</sup> In order to achieve this, ruthenium particles were deposited on a mesoporous silica support (Ru/mSiO<sub>2</sub>) and contacted with the carbon precursor (toluene) at 900 °C in an argon stream. The silica template was then removed by HF etching to obtain Ru nanoparticles inside the hollow carbon spheres (Ru@ HCS), which leaves an interior space that acts as a nanoreactor. Although the high thermal treatment associated with the CVD process led to a wide distribution of Ru particle size (1-13 nm) and low dispersion of 11.1% determined by H<sub>2</sub> pulse chemisorption studies, thermogravimetric analysis (TGA) in air revealed high thermal stability with the onset of decomposition only above 400 °C. This coated catalyst was tested for the Fischer-Tropsch reaction with a classical H<sub>2</sub>/ CO = 2 ratio. The catalyst exhibited good activity with a CO conversion of 6.9, 10.1, and 17.6% at reaction temperatures of 190, 220, and 250 °C, respectively. The authors also investigated another method based on resorcinol/formaldehyde (Ru@MHCS) to overcoat the catalyst. Resorcinolformaldehyde resins are promising carbon precursors for soft-templating synthesis in the preparation of ordered mesoporous carbons because resorcinol reacts with formaldehyde to form a cross-linked backbone with a hydrogenbinding network.<sup>23</sup> It was observed that the Ru@MHCS catalyst displayed a better dispersion (26.9%), improved porosity, and narrower size distribution (2-6 nm), ultimately leading to enhancement in catalytic activity, as shown in Figure 2. These catalysts were very stable under reaction conditions, and no substantial Ru sintering took place below 220 °C.

Though CVD has allowed for effective deposition of overlayers on metal nanoparticles, its wide application for protecting catalysts from deactivation has been limited. This is predominantly attributed to the fact that CVD leads to the formation of thick and nonconformal layers on catalytic surfaces, which invariably impairs the catalytic activity. Ultimately, there lies a difficulty in controlling the thickness of the CVD coating, a challenge that has led to the exploration of other encapsulation techniques.

# 3. ATOMIC LAYER DEPOSITION (ALD)

Atomic layer deposition (ALD) is a technique that has been utilized in the past few decades in large industrial applications ranging from fuel cell applications, <sup>24,25</sup> electrochemical reactions, <sup>26</sup> lubricating coatings, <sup>27</sup> nanostructure materials, <sup>28</sup> and catalysis. <sup>29</sup> ALD is a variation of chemical vapor deposition (CVD), in which a series of self-limiting reactions is employed to deposit metals, metal oxides, and other materials on the surface of a substrate. <sup>30</sup> ALD generally involves exposing the substrate to alternating pulses of different precursors containing the constituent elements for the layers. <sup>31,32</sup> The alternating pulses are separated by a purging inert gas stream to remove the unreacted precursors and volatile byproducts. <sup>29,33–35</sup>

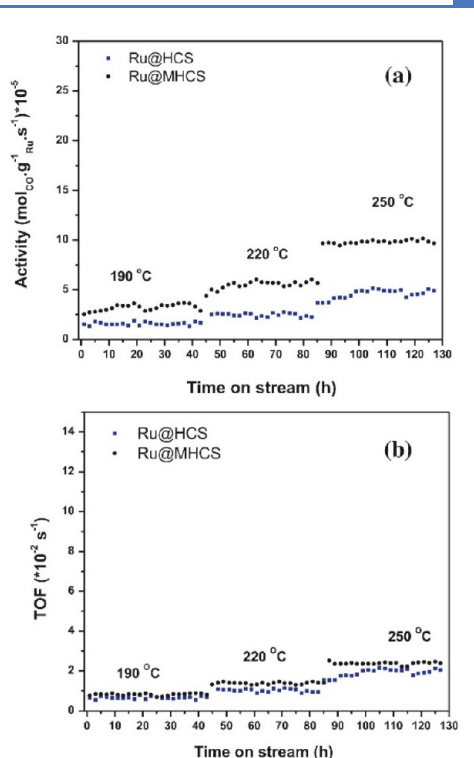


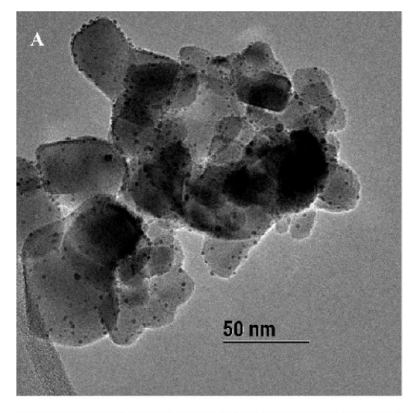
**Figure 2.** Catalytic performance of the Ru@HCS and Ru@MHCS catalysts: (a) Fischer—Tropsch activity and (b) Turnover frequency during 130 h of time on stream. <sup>22</sup> Reproduced with permission from ref 22. Copyright 2016, Elsevier.

The controllable nature of the ALD process has led to its use in the preparation of different catalytic materials, modification of supports, introduction of promoters, and synthesis of active phases. 11 The advantage of ALD over conventional catalyst synthesis methods, such as impregnation and precipitation, include uniform composition, lower contamination from residual salts, monodisperse size, and the ability to penetrate highly porous supports. 11 A good example of improved activity by ALD synthesis was demonstrated by Yan et al., who reported the deposition of single-atom Pd on graphene via ALD. The presence of single atoms induced superior catalytic activity in the selective hydrogenation of 1,3-butadiene, obtaining a 100% selectivity to butene and the highest ever 1-butene selectivity of 70% at a conversion of 95% under mild temperature conditions (50 °C).36 The catalyst was also reported to be durable and stable against deactivation via metallic atom aggregation or carbonaceous deposits during 100 h of time on stream.

In recent times, ALD has also been used to control the deactivation of heterogeneous catalysts by creating an overcoating layer over the surface. ALD has generated increased interest because, unlike other encapsulation techniques, such as CVD and sol—gel chemistry applied to form core—shell structures, it allows for precise control of the thickness and composition of the layer overcoating the catalyst. This allows for control of the metal particle size and conformal deposition of very thin layers, which alleviates problems related to mass transfer resistance.

The use of ALD overcoating to improve the stability of catalysts was first reported by Ma et al.,<sup>37</sup> who used SiO<sub>2</sub> to stabilize titania-supported gold nanoparticles (Au/TiO<sub>2</sub>) from sintering. Gold is a metal that has been extensively studied and

has demonstrated excellent catalytic activity in different reactions; however, its activity has been observed to decrease pronouncedly with increasing particle size, being inactive in its bulk state. Hence, Ma et al. Personant to alternating pulses of tetramethyl orthosilicate (TMOS) and water vapor under vacuum conditions and a temperature of 150 °C. TEM images of the as-synthesized  $SiO_2/Au/TiO_2$  catalyst showed effective decoration of the Au particles with amorphous  $SiO_2$  (Figure 3). The stability of the coated catalyst



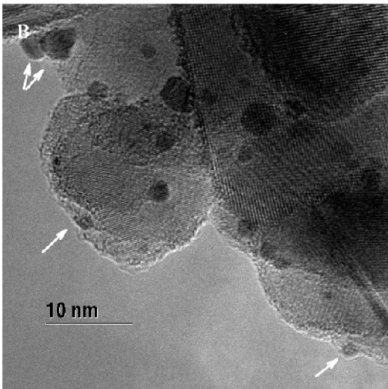


**Figure 3.** TEM images of the SiO<sub>2</sub>-encapsulated Au/TiO<sub>2</sub> catalyst.<sup>37</sup> Reproduced with permission from ref 37. Copyright 2008 American Chemical Society.

was studied on CO oxidation and  $H_2$  oxidation reactions in a plug flow microreactor. Although sintering was successfully limited by the addition of the silica overcoating layer at high-temperature pretreatment conditions, the silica-coated catalyst exhibited less activity than the parent  $Au/TiO_2$  catalysts at lower reaction temperatures. This was attributed in part to the presence of residual organic moieties on the gold surface, limiting the accessibility to the reacting molecules, a hindrance somewhat improved by treating the silica-coated catalyst at higher temperatures before reaction. These findings eventually paved the way for more extensive reports in the use of ALD to control catalyst deactivation.

Instead of using silica to coat gold particles via ALD, Biener et al. reported that alumina and titania ALD films could also be used to stabilize nanoporous gold (np-Au) against sintering. The precursors employed were trimethylaluminum (AlMe $_3$ / H $_2$ O) at 125 °C and titanium tetrachloride (TiCl $_4$ /H $_2$ O) at 110 °C for alumina and titania ALD, respectively. The mechanical properties, such as the strength and stiffness of the material, were also observed to improve markedly. They found that a 1 nm thick alumina ALD layer was able to

stabilize np-Au up to 1000 °C, while a ~6 nm alumina layer led to a 7- and a 3-fold improvement in the hardness and Young's modulus, respectively. The thermal stability of titania-coated particles was found to be lower than that of the alumina-coated gold particles. Catalytic tests performed on the titania ALD coated np-Au using the oxidation of CO showed improvements when compare to pristine np-Au. Prior to the reaction, the coated catalyst was annealed at 600 °C to create pores in the titania overcoat. The titania-coated catalyst exhibited a 3-fold increase in the catalytic activity, which depicted an added effect of the ALD titania catalyst to the uncoated np-Au. Unsurprisingly, annealing the uncoated np-Au at 600 °C led to a 50% drop off in the reactivity that can be attributed to sintering and loss of active surface area. This marks a case where ALD was used to improve both catalyst stability and activity.

Feng et al. reported the stabilization of Pd nanoparticles toward the methanol decomposition reaction at high temperature. 40 Although these researchers had previously synthesized Pd and Ru-Pt catalysts using ALD, this was the first time they used this technique to overcoat a catalyst to protect it against deactivation. 41 First, Pd nanoparticles were supported on Al<sub>2</sub>O<sub>3</sub>-coated silica gel by ALD, then an aluminum oxide protective layer was deposited onto the catalyst. The ALD alumina deposition was carried out by using alternating exposures to trimethylaluminum (TMA) and deionized water at a temperature of 200 °C. Different samples comprising 1, 2, 4, 8, 12, 20, 24, and 32 cycles of Al<sub>2</sub>O<sub>3</sub> ALD were prepared on both the metallic Pd catalyst and the bare support. 40 A linear relationship between the number of cycles and the relative sample weight gain was observed, demonstrating a uniform addition of the overcoat layer after each cycle. The average thickness per cycle on the catalyst was evaluated to be 0.8 Å, while the average increase on the bare support was slightly higher than  $\sim 1.0$  Å/cycle as a result of the interaction between TMA and surface hydroxyl groups on the  $Al_2O_3$ . The methanol decomposition reaction was used to evaluate the effect of the Al<sub>2</sub>O<sub>3</sub> ALD overcoat on the catalyst reactivity. The activity of the catalysts with 1 to 16 cycles of alumina overcoating was considerably higher than that of the uncoated catalyst, as sintering was evident on the latter. However, the catalytic activity decreased progressively beyond the 16 cycles, with the 32 cycles coated catalyst showing the least activity, because the overlayer presented a greater barrier for reactants to diffuse to the active sites. It was also observed that the Al<sub>2</sub>O<sub>3</sub> ALD overcoats preferentially nucleate at the corners, edges, and steps of the Pd nanoparticles, thereby leaving the active Pd (111) facets available for methanol decomposition. Sintering at elevated temperatures was also investigated using the bare and the 16 cycles coated catalyst heated at 500 °C in Ar for a period of 6 h. While STEM images showed a significant presence of large particles (10-20 nm) on the used bare Pd catalyst, only small particles were observed on the 16 cycles Al<sub>2</sub>O<sub>3</sub> ALD overcoated catalyst, indicating that sintering was avoided.

Similarly, Lu et al. showed that Al<sub>2</sub>O<sub>3</sub> ALD overcoating was able to protect Pd catalysts from both sintering and coking during the high-temperature oxidative dehydrogenation of ethane to ethylene.<sup>42</sup> The reaction was performed at 675 °C, and it was observed that 45 ALD cycles were enough to stabilize the catalyst fully. TGA of the ALD coated catalyst revealed less than 6% of the coke formed on the uncoated catalyst, and STEM images showed no changes in the

morphology after 28 h of reaction. There was also an improved yield of ethylene on the ALD overcoated catalyst. Upon encapsulation, CO chemisorption studies indicated complete coverage of the Pd particles. In order to restore the accessibility to the Pd nanoparticles, the overcoated catalyst was calcined at 700 °C for 2 h under 10% O $_2$ /He flow and subsequently reduced in 5% H $_2$ /He at 300 °C. This created pores in the overcoating layer and restored the accessibility to the active sites, with BET analysis indicating 84% restoration of the catalyst surface area. The authors concluded that the exceptional resistance to sintering and coking might be due to the selective blockage of edge and corner atoms by alumina overcoats.

In 2015, Onn et al. used a different metal oxide, zirconia (ZrO<sub>2</sub>) to stabilize an alumina-supported palladium oxide (PdO/Al<sub>2</sub>O<sub>3</sub>) catalyst. 43 The ZrO<sub>2</sub>-coated catalyst was calcined at 500 and 700 °C, and methane oxidation was used as a probe reaction to evaluate the effect of the zirconia film on the catalytic activity of the PdO/Al<sub>2</sub>O<sub>3</sub> catalyst. The zirconia layer was found to stabilize the PdO particles against sintering in air at 800 °C, and the catalyst exhibited an increased catalytic activity. Interestingly, it was observed that ZrO<sub>2</sub> could only grow on PdO and not on Pd, suggesting that ALD could be used to induce a promotional effect on metal catalysts. It was postulated that PdO must be present in the active phase and that sintering was more severe when PdO decomposed to Pd (which normally occurs at temperatures >800 °C). Although the mechanism by which the zirconia layer protected the catalyst was unclear, they suggested that the ZrO<sub>2</sub> films could stabilize the PdO phase or simply create a physical barrier that prevented sintering.

ALD has also shown great potential to protect non-noble metal catalysts, which are more prone to deactivation. A similar approach to Lu's was employed by O'Neill et al. to stabilize copper nanoparticles supported on γ-Al<sub>2</sub>O<sub>3</sub> for the liquid-phase hydrogenation of furfural.<sup>44</sup> This work was the first reporting the use of ALD to stabilize a base metal for liquid-phase reactions. 45 cycles of alternative exposures to trimethylaluminum and water were utilized to overcoat the catalyst, and this was treated at 700 °C to create pores that enabled the access of reactant molecules to the active sites. This catalyst was compared with a bare  $Cu/\gamma$ -Al<sub>2</sub>O<sub>3</sub> catalyst in the liquidphase hydrogenation of furfural to furfuryl alcohol in 1-butanol at 130 °C and 22 bar. As the reaction progressed, both catalysts experienced a loss in catalytic activity. Whereas the activity of the bare copper catalyst was not fully recovered after calcination, the activity of the overcoated catalyst was fully recovered, which confirmed that the encapsulation protected the catalyst from leaching and sintering. As these modes of deactivation are believed to initiate from undercoordinated copper atoms, the stability induced by the alumina ALD layer was attributed to the preferential coverage of the undercoordinated sites (e.g., steps, edges, and corners) that remain covered after pore opening, while most terraces are exposed after annealing (Figure 4). Coking, however, was experienced in both coated and uncoated catalysts, as it could be inferred from the initial loss of catalytic activity. Since the acidity of the overcoat was suspected to be responsible for the coke formation, O'Neill et al. decided to vary the number of Al<sub>2</sub>O<sub>3</sub> ALD cycles and modify the overcoat with basic MgO<sub>x</sub> in order to reduce its acidity.45 It was observed that decreasing the number of ALD cycles from 45 to 5 increased the rate per gram of catalyst and reduced the rate of deactivation for the

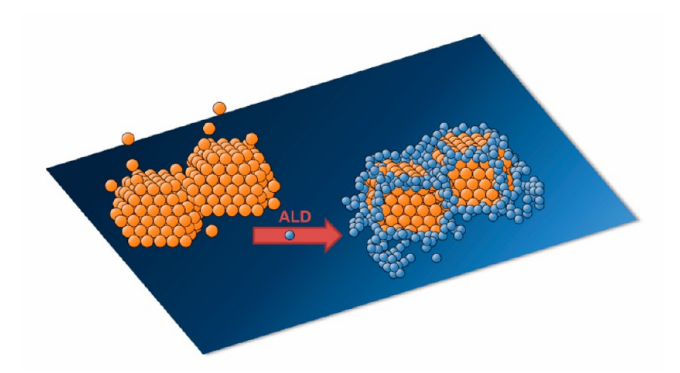


**Figure 4.** ALD protection on metallic nanoparticles. <sup>44</sup> Reproduced with permission from ref 44. Copyright 2013, Elsevier.

catalyst pretreated at 400 °C. In addition, it was concluded that even when the modification with  ${\rm MgO}_x$  was not able to prevent the deactivation completely, it contributed to decreasing the acidity and the deactivation rate through coking. They observed that a catalyst containing 10 cycles of  ${\rm MgO}_x$  overcoat and 5 cycles of  ${\rm Al}_2{\rm O}_3$  ALD yielded a deactivation rate nearly 3 times lower than the 45 cycles  ${\rm Al}_2{\rm O}_3$  ALD catalyst previously reported.<sup>44</sup>

The stability of a copper chromite (CuCr<sub>2</sub>O<sub>4</sub>·CuO) catalyst for the selective gas-phase hydrogenation of furfural was also enhanced by depositing alumina using ALD by Zhang et al. deposited to investigate the effectiveness of the method to improve the catalyst stability without impairment of activity (Figure 5). Each catalyst was pretreated at 700 °C to induce

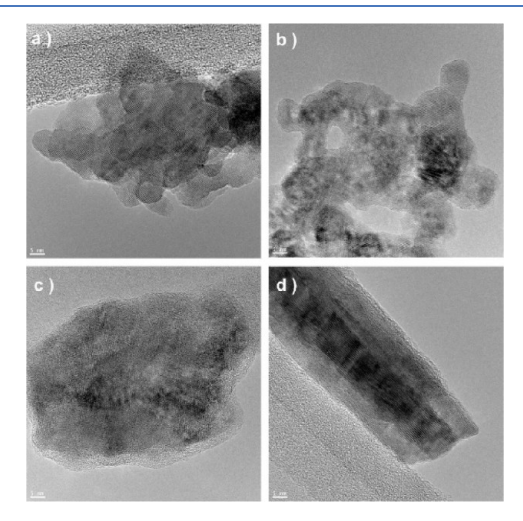


**Figure 5.** TEM images of (a) Cu-chromite, (b) Cu-chromite-10 cycles alumina ALD, (c) Cu-chromite-20 cycles alumina ALD, and (d) Cu-chromite-45 cycles alumina ALD. AED. Reproduced with permission from ref 46. Copyright 2014 Elsevier.

porosity prior to reaction. Conversely to earlier reported work, in which 1 cycle of  ${\rm Al_2O_3}$  ALD was able to effectively prevent Pd nanoparticles from sintering, <sup>40</sup> the 10-cycle ALD coating provided limited stability for the Cu-chromite catalyst. Higher loadings were able to improve stability but led to a reduction in catalyst activity. These authors concluded that the alumina overcoating layer was able to reduce the coke formation, copper sintering, and coverage of the copper sites by chromite migration. In addition, the ALD overcoat increased the

reduction temperature of copper and reduced the activation energy for the hydrogenation of furfural. Later on, Zhang et al. also carried out comparative studies with TiO<sub>2</sub> and Al<sub>2</sub>O<sub>3</sub> ALD overcoat on the copper chromite catalyst for the same reaction. Twenty cycles of TiO2-ALD coated catalyst was found to retain about 75% of the Cu-chromite initial catalytic activity after 10 h on stream, this being much higher than the bare Cuchromite, which only retained less than 20% of its initial activity after the same exposure time. The TiO2-ALD catalyst also performed much better than the Al<sub>2</sub>O<sub>3</sub>-ALD coated catalyst, which only regained 30 and 10% of the Cu-chromite initial activity for 10 and 45 ALD cycles, respectively.<sup>47</sup> Upon calcination at 500 °C, the TiO2 overcoat showed fewer modification effects on the base catalyst when compared with the ALD alumina overcoat, and therefore, it did not strongly impair the activity of copper as in the case of the ALD alumina catalyst.

At this point, the reader might be questioning the use of alumina ALD to provide stability to the catalysts since alumina is not stable under hydrothermal conditions. In fact, the CVD section included an example in which graphitic carbon was used to stabilize an alumina support (gc-Al<sub>2</sub>O<sub>3</sub>).<sup>21</sup> The stability of alumina ALD can been attributed to its densification and crystallization upon annealing at high temperature, <sup>48</sup> which is also an essential step for the creation of pores on the overcoating layer.

 ${
m TiO_2}$  ALD was also employed by Lee et al. to stabilize cobalt catalysts for APH reactions, preventing leaching and sintering of the cobalt nanoparticles. An uncoated cobalt catalyst was observed to leach and sinter under the same conditions. The authors speculated that the stability of the titania-coated cobalt catalyst was due to the decoration of undercoordinated cobalt sites located at defects, corners, and edges, where leaching and sintering begin. When  ${
m Al_2O_3}$  was used as the overcoating layer, there was a complete loss in catalytic activity owing to the formation of an irreducible cobalt aluminate phase. However, the ALD  ${
m TiO_2}$ -coated cobalt catalyst was active for APH of a variety of feedstock, including furfuryl alcohol, furfural, and xylose.

While ALD is primarily employed for inorganic coating, a recent variant of this technique called molecular layer deposition (MLD) is being employed over metal catalysts to produce hybrid organic-inorganic or fully organic layers depending on if one or both reactants are organic compounds. 50 MLD is a vapor-phase deposition technique that utilizes a layer-by-layer approach with two alternating surface reactions. 51 Like ALD, MLD precursors need to be volatile, reactive, and thermally stable at the reaction conditions to ensure feasible film growth. 50 Liang et al. reported the use of MLD to encapsulate a Pt catalyst with an ultrathin highly porous film.51° Alternating reactions of trimethylaluminum (TMA) and ethylene glycol (EG) were employed to form aluminum alkoxide (alucone). This is described as an "AB" type MLD chemistry with TMA (precursor A) and ethylene glycol (precursor B). The thin films were produced by oxidizing the alucone hybrid polymer. The Pt particles were totally covered after 20 MLD cycles, and their stability was evaluated at 400, 600, and 800 °C for 4 h in air, obtaining the dispersions shown in Table 1. Even though the bare catalyst (no MLD overcoating) initially had the highest dispersion, this dramatically decreased after heating up to 600 and 800 °C. However, MLD clearly improved the stability of the catalysts, especially after 40 cycles. The

Table 1. Dispersion Measurements for Pt/SiO<sub>2</sub> with MLD Overcoating after Thermal Treatment.<sup>51</sup> Reprinted with Permission from Ref 51. Copyright 2011 American Chemical Society

		number of MLD cycles				
	temperature, °C	0	10	20	30	40
Pt dispersion, %		65	42	37	38	38
	400	59	42	48	43	42
	600	12	37	42	39	43
	800	3.9	10	27	25	34

reactivity of the catalysts was studied using the CO oxidation reaction. It was observed that the porous coating decreased the activity of the catalyst, and hence, higher temperatures were required to attain full CO oxidation, likely because of the small size of the pores limiting reactant accessibility. Interestingly, the authors observed that the 20 MLD cycle catalyst calcined at 800 °C was less active than the catalyst calcined at 600 °C, a phenomenon attributed to the crystallization of the alumina layer to form  $\gamma$ -alumina.

MLD technique was also used by Gould et al. to stabilize Ni catalysts.<sup>52</sup> These authors encapsulated the catalysts by growing alumina via "ABC" type MLD chemistry of alucone, using TMA (precursor A), ethanolamine (precursor B), and maleic anhydride (precursor C). This ABC alucone MLD created a thicker layer with a high organic fraction when compared to the AB alucone MLD reported by Liang et al.<sup>51</sup> Because the organic component was removed upon calcination, this ABC type layer produced larger pores (0.8 nm) when compared with AB alucone MLD (0.6 nm). Here, a Ni catalyst was synthesized by ALD on an Al<sub>2</sub>O<sub>3</sub> support, after which the polymer-inorganic alucone MLD layer was deposited to stabilize the catalyst. This created an organic-metallic overlayer on the catalyst. Calcination of the MLD-modified catalyst was carried out in 20% O<sub>2</sub> at 500 °C to create pores in the alumina overcoat, and the catalysts were studied in the dry reforming of methane (DRM) reaction at 700 °C. While the reaction rate was found to increase over time until stabilization for the MLD-modified catalyst, the activity with the uncoated catalyst decreased over time due to sintering and coking. The MLD overcoating layer prevented the catalyst from sintering, and a calcination step was enough to regenerate the catalyst. The 5-MLD cycles sample yielded the highest DRM rate (even higher than the uncoated catalyst after 6 h). In contrast, the 10-MLD cycles catalyst was found to be the most stable after repeated calcinations and reductions, being operated for long hours on stream without noticeable deactivation.

A hybrid of MLD and ALD was reported by Goulas et al. <sup>53</sup> for the production of ultrathin aluminum-based overcoats on a supported platinum catalyst. In this work, they made use of a fluidized bed reactor operating at atmospheric pressure. Al<sub>2</sub>O<sub>3</sub> ALD was conducted using TMA and water at 120 °C. The hybrid ALD/MLD alucone was performed using a diolethylene glycol (EG) or 1,5 pentanediol (PD)— along with TMA. The use of diols in place of water was observed to lead to lower growth of the protective films. The catalyst was subjected to 15 cycles of overcoat and calcined at 800 °C to create pores in the overcoating layer. From total adsorption studies, it was found that the calcination of the catalyst improved the accessibility; however, CO chemisorption experiments indicated that only ~25% of the Pt clusters were still accessible. This was suggested to be the result of the

#### Coating of high surface area materials by subsequent stoichiometric injections

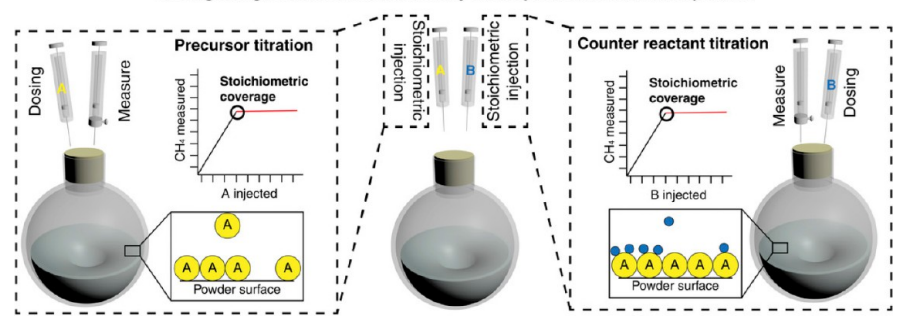


Figure 6. General set up for liquid-phase ALD.<sup>57</sup> Reproduced with permission from ref 57. Copyright 2019, John Wiley and Sons.

densification of the  $AlO_x$  phase. The authors were able to elucidate the effect of the coreactant choice (water, ethylene glycol, and 1,5-pentanediol), and the use of fluidized bed reactors improved the prospect of large-scale implementation of the ALD technique.

Yi et al. reported an enhanced selectivity and durability using a porous alumina ALD overcoat on Pd catalysts for the hydrogenation of 1,3-butadiene. The overcoat was found to improve the selectivity to butenes, and the overcoated catalyst also exhibited excellent durability against catalyst deactivation after 124 h of time on stream. More recently, Kennedy et al. replicated the strong metal—support interaction (SMSI) effect using ALD of titania on supported platinum nanoparticles. Using the hydrogenation of acrolein as a probe reaction, they observed that the TiO<sub>2</sub> ALD catalyst increased the selectivity to allyl alcohol from 2.9 to 13.9%. The improvement of the selectivity, alongside an observed preferential growth of the titania ALD overcoat on the platinum nanoparticles, were indicative of a behavior similar to SMSI.

While all these examples used ALD in the gas phase (associated with expensive precursors, extensive purging, and high vacuum), Héroguel et al. developed a novel layer-by-layer approach in liquid medium to deposit conformal alumina overcoats for control of catalyst deactivation. 56 In this method, the metal oxide precursor and water are contacted on the substrate in stoichiometric amounts. This prevents side reactions and the purging of excess precursors, a common feature in gas-phase ALD. Alternate exposures of the catalyst surface to stoichiometric quantities of aluminum alkoxide and water in liquid phase produce very tunable porous overcoats. Sixty cycles of alumina were used to stabilize a Cu/Al<sub>2</sub>O<sub>3</sub> catalyst against leaching and sintering during the liquid-phase hydrogenation of furfural. This technique is very sensitive to changes in synthesis parameters, and it can be modified to improve the porosity of the overcoat and accessibility to the metal sites, providing control of the overcoat nanoarchitecture that is lacking in gas-phase synthesis. It should be mentioned that the effectiveness of this technique lies in the accurate determination of the stoichiometric amount of the precursors, as an excess would lead to the onset of heterogeneous nucleation, creating an additional support and diluting the active sites. On the other hand, an insufficient amount would leave the metal surface exposed and unprotected.<sup>56</sup> More recently, the same research group conducted comparative studies between conventional gas-phase ALD and liquid-phase ALD.<sup>57</sup> The general setup for the liquid-phase ALD is depicted in Figure 6. Here, stoichiometric quantities of TMA (typical ALD precursor) and water were added sequentially on silica spheres, and the progress of the reaction was monitored in situ

on the basis of the amount of methane released during the process. The coating quality and conformality were identical to that obtained by conventional gas-phase ALD performed in a fluidized bed reactor; however, interestingly, the liquid-phase ALD overlayer was thinner (1.5 nm vs 3 nm). Another interesting feature of the liquid-phase ALD process was the potential for scale-up, with 158 g of coated silica prepared under the same conditions in a bigger flask. The researchers were also able to use this technique to deposit phosphates, a process that requires three precursors and six steps to complete in conventional ALD. Finally, the authors used this method to coat a Pd catalyst with alumina, preventing its sintering after thermal treatment. Thus, they effectively showed the efficacy of this technique for both noble and non-noble metals.

ALD encapsulation usually involves a calcination step to create pores in the overcoating layer for access of the reactants to the active sites; however, not much work has focused on the study of the mechanism of the pore formation. In an effort to characterize the pores formed during ALD, Alba-Rubio et al. coated a Cu/spherical silica catalyst with 30 cycles of alumina ALD and calcined it at 700 °C (Figure 7). The authors found a method to indirectly image the pores by filling them with niobium oxide using 20 cycles of ALD. By using scanning

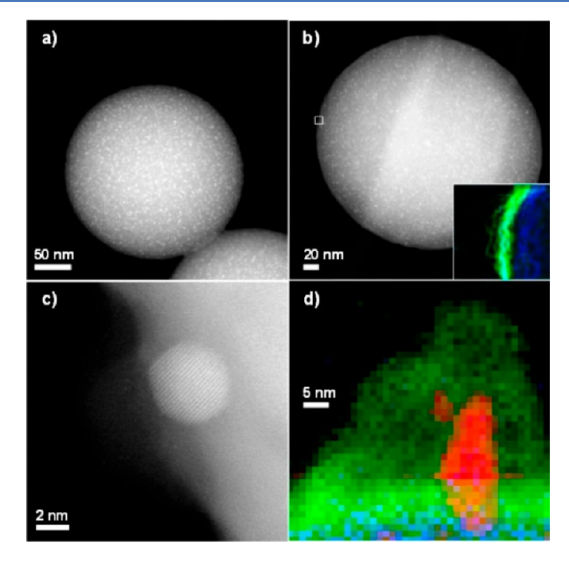


**Figure 7.** STEM imaging of (a) Cu/spSiO<sub>2</sub> reduced, (b) 30 ALD  $AlO_x/Cu/spSiO_2$  (including EDS map of the border), (c) 30 ALD  $AlO_x/Cu/spSiO_2$ , showing aluminum oxide-coated Cu particle, and (d) EELS map of coated Cu nanoparticle. Colors and element correspondence: green, Al; blue, Si; red, Cu. Se Reproduced with permission from ref 58. Copyright 2014 American Chemical Society.

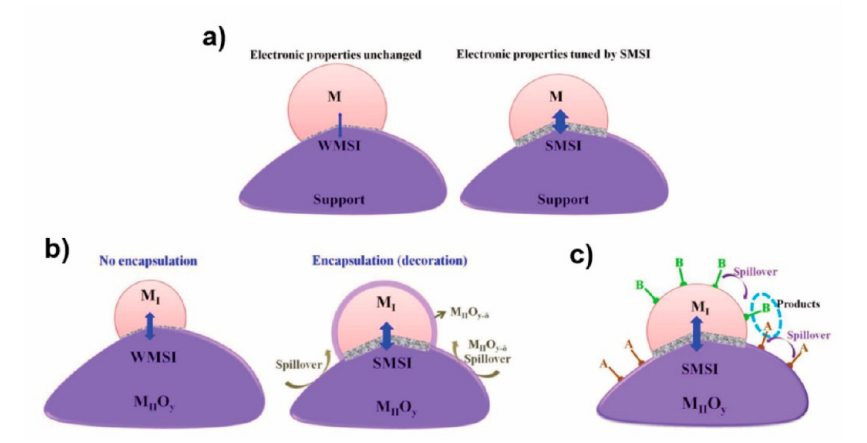


Figure 8. Fundamental effects associated with SMSI: (a) electronic effect, (b) geometric effect, and (c) bifunctional effect. <sup>12</sup> Reproduced with permission from ref 12. Copyright 2017 Elsevier.

transmission electron microscopy/electron energy loss spectroscopy (STEM/EELS), they concluded that the size of the pores was ~1 nm, information that was also confirmed by small-angle X-ray scattering (SAXS). These catalysts were studied in the liquid-phase hydrogenation of furfural to furfuryl alcohol, and the overcoating layer proved to protect the catalyst from deactivation. It was also established that the addition of niobia to the stabilized overcoated catalyst provided metal-acid bifunctional properties.

Afterward, Li et al. explored the mechanism of pore formation in ALD overlayers using in situ small-angle (SAXS) and wide-angle X-ray scattering (WAXS).<sup>59</sup> They concluded that the pores were induced by the high-temperature annealing of the samples, a phenomenon attributed to the densification of the ALD overlayer as a result of a phase transition from amorphous to crystalline. In addition, the size of the pores was observed to increase with increasing temperature.

Although ALD allows for deposition of conformal thin layers (<10 nm) and has been used extensively to tune properties at the molecular level, one major challenge is the cost associated with ALD applications. The extensive use of vacuum and relatively high temperatures require the use of highly specialized equipment, which are quite expensive.<sup>31</sup> In addition, high-purity substrates are essential, making the industrial application highly limited. 10 ALD has also been known to suffer from slow deposition rates as a result of prolonged cycle times involved in pulsing and purging the precursors, with most ALD rates being of 100-300 nm·h<sup>-1</sup>.60 Another challenge associated with the practical application of ALD in catalysis is the technical difficulties associated with scaling up the process. However, the application and commercialization of ALD in the microelectronics industry show that this problem might be resolvable once the ALD synthesis gains initial adoption in the catalysis market.<sup>31</sup> The interesting prospect of implementing ALD in the liquid phase bodes well for effective scale-up and industrial application. This liquid process has an added advantage, as it can be conducted at room temperature and pressure, hence limiting the energy requirement. In addition, this process makes use of less expensive precursors, and the introduction in stoichiometric quantities limits excess usage and purging.

## 4. STRONG METAL-SUPPORT INTERACTION (SMSI)

The term strong metal-support interaction (SMSI) was introduced in the late 1970s to explain the observed effects on the chemisorption properties of the Group VIII noble metals when supported on titanium oxide. 61 Tauster et al. observed that the chemisorption properties of noble metals were greatly affected by the interactions with the TiO2 support.<sup>62</sup> In further studies, they demonstrated that different metals form interfacial bonds with surfaces of reduced transitional metal oxides, such as titanium, niobium, manganese, tantalum, and lanthanum oxides. 61,63 These interactions, postulated to occur at high reduction temperatures, are marked by a migration of the oxide support leading to coverage of the metal surface. 63,64 Interestingly, some recent reports have also indicated that the SMSI effect can occur at low temperatures.<sup>65</sup> The main features of classical SMSI are migration of the support accompanied by the creation of a thin overlayer on the supported metal, significant suppression of CO and H<sub>2</sub> adsorption, transfer of electrons from support to the metal, and a subsequent reversal of these effects upon reoxidation.66

Pan et al. explained three fundamental effects associated with SMSI: electronic, geometric, and bifunctional effects. 12 The schematic of these three effects is shown in Figure 8. The electronic effect refers to the charge redistribution that occurs on the interface between a metal and an oxide support and is governed by principles such as energy minimization. This determines the electron transfer that occurs along with the breaking and formation of new chemical bonds. The effect on the electronic structure is less significant if the interaction is weak, as in the case of weak metal-support interaction (WMSI). The geometric effect is the decoration of the metal surface, leading to partial coverage or total encapsulation of the metal by the support. This also involves morphological changes that occur on the catalyst as a result of the metal-support interactions; in some cases, the metal particles can be flattened (for smaller particles), while in other cases, the metal particles are unaffected. The bifunctional effect involves the creation of new reaction sites at the interface between the metal and the support, providing a synergistic effect and improving catalyst activity and selectivity. This also encompasses the spillover phenomenon in which reactants migrate from metal or support and reacts at the interface.

X-ray photoelectron spectroscopy (XPS) analysis carried out by Sexton et al. on metals supported on different oxides revealed the reduction of the supports associated with the SMSI effect.<sup>67</sup> These authors were able to show evidence of the SMSI effect on rhodium and platinum particles supported on different transition metal oxides (TiO<sub>2</sub>, V<sub>2</sub>O<sub>5</sub>, Ta<sub>2</sub>O<sub>5</sub>, Nb<sub>2</sub>O<sub>5</sub>, and HfO<sub>2</sub>). The hydrogen spillover effect was also confirmed on Pt/TiO<sub>2</sub> catalysts, with a reduction of the titania support between 400 and 500 °C, which is lower than that obtained for pure titania (>550 °C), indicating a more facile reduction process. The presence of oxygen vacancies as a result of the SMSI effect was modeled by Sánchez and Gázquez.<sup>68</sup> Baker et al. studied platinum particles on different supports (carbon, aluminum oxide, silicon oxide, and titania) from 50 to 800 °C, <sup>69,70</sup> and concluded that the stability of platinum was higher on a titania support, a characteristic that was attributed to the SMSI effect. Gao et al.<sup>71</sup> reported that the presence of Nb doping on TiO<sub>2</sub> occupied the oxygen vacancies suppressing the diffusion and encapsulation of Pt metal by the support, indicating that Nb-doping limits the SMSI effect on titania support.

Fu et al. demonstrated the use of SMSI to develop a Pd/ $CeO_2/C$  catalyst with high resistance to leaching.<sup>72</sup> In this work, they established that the electron transfer from the carbon support via the  $CeO_2$  to the Pd particles provided excellent leaching resistance to the Pd catalyst. This, along with the transfer of oxygen from the ceria, improved the stability and activity of the catalyst for the catalytic wet air oxidation of  $N_1N$ -dimethylformamide (DMF).

Tang et al. described the SMSI effect between gold nanoparticles and hydroxyapatite (HAP), the first example of SMSI between a metal and a nonoxide support. The gold nanoparticles were encapsulated by HAP, the extent of the coating being dependent on the temperature of calcination. The Au/HAP catalyst was subjected to different calcination temperatures from 200 to 600 °C in air for 3 h, and the morphological changes are depicted in Figure 9. It was observed that the encapsulation of the Au nanoparticles only occurred at calcination temperatures ≥300 °C, with the degree of coverage increasing progressively as the calcination temperature increased until reaching complete coverage at 600 °C. Further analysis by EELS corroborated that the

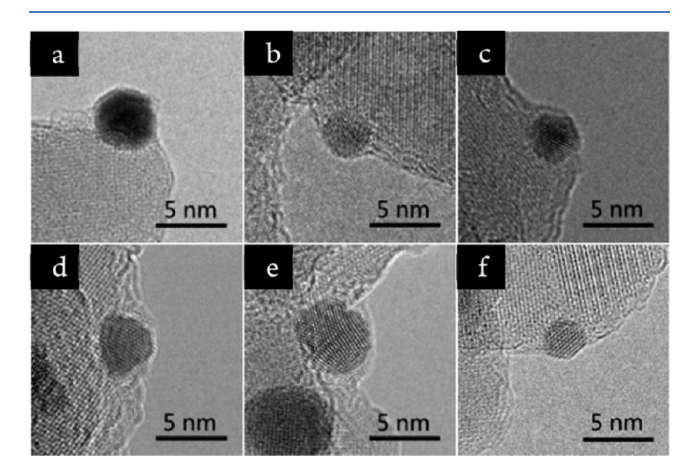


**Figure 9.** HRTEM images of (a) Au/H-200, (b) Au/H-300, (c) Au/H-400, (d) Au/H-500, (e) Au/H-600, and (f) Au/H-500-H<sub>2</sub>. Reproduced with permission from ref 73. Copyright 2016 American Chemical Society.

coating overlayer was originated from the HAP support, a characteristic feature of SMSI. Unlike the conventional reductive method, this reversible encapsulation took place under oxidative conditions. When CO oxidation was used as a probe reaction, a reduction in the activity was observed with increasing calcination temperature, which was attributed to the decreased exposure of gold active sites as a result of the increasing HAP overlayer. Even though the SMSI-induced layer reduced the catalytic activity of the catalyst, it was shown that the coated catalysts (Au/H-300-600) had smaller particle size and better activity than the uncoated catalyst (Au/H-200). This proved that the SMSI overlayer was effective in preventing sintering during the CO oxidation studies. The coated (Au/H-500) and uncoated catalysts (Au/H-200) were also tested in the liquid-phase conversion of benzyl alcohol to benzaldehyde. While the uncoated catalyst exhibited a loss of activity after 2 cycles due to leaching and sintering, the coated catalyst was stable and maintained its conversion and selectivity to benzaldehyde after 5 cycles. The authors also reported that this SMSI effect could be extended to other phosphate-supported gold catalysts due to the generality of the

In order to modify the SMSI effect on Au/HAP, Tang et al. decided to alter the support by introducing titania. They observed that by adding TiO2, Au nanoparticles occupied the interfacial region between the support materials leading to partial encapsulation. Remarkably, this catalyst was very stable against sintering after calcination at 800 °C and showed excellent activity in CO oxidation studies. The partial coverage of the Au nanoparticles by HAP was primarily responsible for the high stability, while the proximity of the Au surface to TiO<sub>2</sub>. enhanced the catalytic activity. This introduced a new concept for tuning SMSI behavior on supported metals. Further, Tang et al. performed classical SMSI studies involving gold on titania support.66 Prior to this example, classical SMSI had been difficult to achieve on gold catalysts, and they reported the encapsulation of Au nanoparticles with a TiO<sub>x</sub> layer following reductive treatments.<sup>66</sup> The catalyst also showed consistent SMSI attributes, such as suppression of CO adsorption and transfer of electrons from the support to the Au nanoparticles. Similar features were observed when the gold nanoparticles were supported on CeO<sub>2</sub>, and Fe<sub>3</sub>O<sub>4</sub> supports, indicating that gold can exhibit classical SMSI characteristics with other oxides besides TiO<sub>2</sub>.66 They were also able to prove the effectiveness of other group 1B metals (Cu and Ag) to display SMSI characteristics on a TiO2 support.

Another example of the encapsulation of gold nanoparticles by SMSI was provided by Liu et al. when they reported the first case of SMSI between gold and ZnO nanorods.<sup>75</sup> This work also focused on the oxidative SMSI (O-SMSI) mechanism between gold and ZnO nanorods in a Au/ZnO catalytic system. The catalyst was subjected to oxidative conditions at 300 °C and also to conventional reductive SMSI (R-SMSI) at 300 °C with H<sub>2</sub>. The authors observed that the electron transfer between the gold nanoparticles and the support led to the migration of ZnO over the surface of Au with subsequent encapsulation. CO oxidation was used as a probe reaction to elucidate the significance of the O-SMSI effect. Interestingly, they observed that the classical SMSI obtained from reductive treatment (R-SMSI) led to a lower activity for CO oxidation. It was observed that, for the R-SMSI, the electron transfer is from the support to the metal, making gold to sink under ZnO with the formation of AuZn alloy, while in the O-SMSI the electron

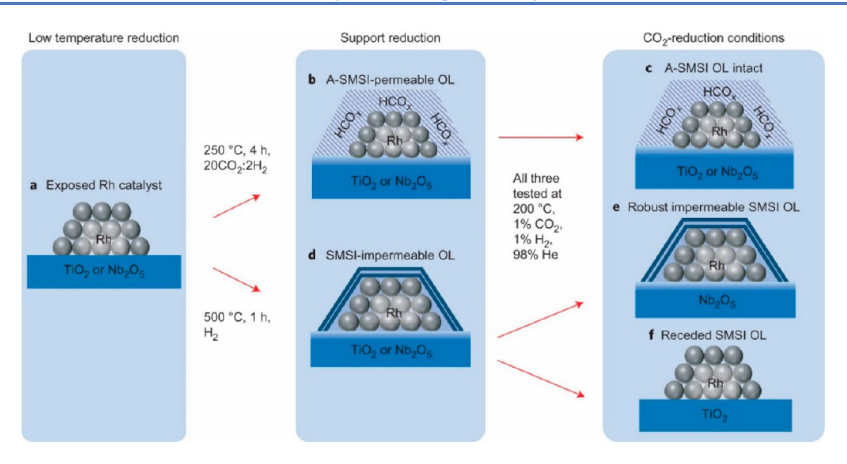


Figure 10. Schematic showing SMSI and A-SMSI effect on supported Rh nanoparticles.<sup>77</sup> Reproduced with permission from ref 77. Copyright 2019 Springer Nature.

transfer is from the metal to the support, facilitating the migration of ZnO onto the gold surface and its encapsulation. They concluded that the O-SMSI had a strong effect on the activity of the catalyst before and after encapsulation. Similarly, Liu et al. encapsulated gold nanoparticles under oxidative SMSI (O-SMSI) conditions.<sup>76</sup> In their work, gold nanoparticles were supported on titania, while melamine (an adsorbate) was used to induce the overlayer formation. The obtained catalyst (Au/TiO<sub>2</sub>@M) was annealed in N<sub>2</sub> at 600 °C and then subjected to calcination experiments at 800 °C for 3 h in air. This strategy increased the strength of the interaction between gold and the titania support, leading to the formation of a thin permeable TiO<sub>x</sub> layer over the gold nanoparticles. Complementary studies suggested that the presence of melamine, pretreatment in N2, and high-temperature calcination in air were all necessary for the formation of the  $TiO_x$  overlayer. Thus, indicating the effectiveness of the adsorbate-mediated approach for oxidative SMSI. Just like in the case of Au on ZnO, the electron transfer was from Au to the TiO<sub>2</sub> support, leading to the reduction of Ti<sup>4+</sup> to Ti<sup>3+</sup> and a partial positive charge on gold with subsequent migration of TiO<sub>x</sub> onto the gold surface and formation of a Au–Ti bond. This catalyst displayed high sintering resistance and exceptional catalytic activity for CO oxidation and water-gas shift reaction. Remarkably, the same phenomenon was observed when Au was supported on two different titania forms: anatase and rutile.

Furthermore, the use of other adsorbate-mediated strong metal-support interactions (A-SMSI) to stabilize oxidesupported rhodium catalysts has been reported. 77,78 The researchers made use of not only TiO2 but also a Nb2O5 support and demonstrated the SMSI encapsulation of Rh particles in a  $CO_2$ - $H_2$  environment. The presence of the  $CO_2$ rich feed drove the migration of HCO<sub>x</sub>-functionalized support over the Rh metal nanoparticles, and the stable A-SMSI layer modified the activity of the Rh particles for CO<sub>2</sub> reduction. As it can be seen in Figure 10, the classical SMSI forms an impermeable overlayer onto the Rh particles, and under the reaction conditions, this stays intact when using Nb<sub>2</sub>O<sub>5</sub> and completely recedes on a TiO<sub>2</sub> support. On the other hand, the A-SMSI of Rh on both TiO<sub>2</sub> and Nb<sub>2</sub>O<sub>5</sub> creates a permeable overlayer around the Rh particles that modifies the catalytic activity. HCO<sub>x</sub> was said to induce oxygen-vacancy on the support, which fostered the formation of the A-SMSI layer. After subjecting the SMSI and A-SMSI Rh/Nb<sub>2</sub>O<sub>5</sub> catalysts to

a feed of  $CO_2$  and  $H_2$ , SMSI caused a blockage of the Rh nanoparticles leaving only isolated Rh atoms to produce CO, while A-SMSI modified the Rh nanoparticles toward producing more CO, indicating the promotional effect of the A-SMSI technique.

While some research groups have focused on ALD to avoid the challenges associated with the high-temperature reductive and oxidative conditions required for the occurrence of the SMSI effect, others have explored different ways to modify the SMSI process while taking advantage of its features. A wet chemistry SMSI (wcSMSI) method for encapsulating gold nanoparticles with a titania support was reported by Zhang et al. 79 Here, the authors made use of an aqueous solution at room temperature, and the driving force behind this idea was the prevention of sintering that occurs during the hightemperature treatments when using conventional SMSI processes. A colloidal TiO<sub>x</sub> solution was contacted with a Au nanoparticle colloid under stirring, after which the suspension was acidified with H2SO4 in a process referred to as a solimmobilization method. Successive drying at 100 and 300 °C was needed to obtain the Au/TiO<sub>x</sub>-wcSMSI catalyst. This wcSMSI TiO<sub>x</sub> layer stabilized the Au nanoparticles against sintering in the CO oxidation reaction.

In another novel SMSI approach, Wang et al. synthesized a catalyst having the SMSI effect without the need for a reduction or oxidation step. They used a hydroxide-to-oxide support transformation to exhibit the SMSI effect between gold nanoparticles and Mg–Al layered double oxides (Au/LDO). To achieve this, a Mg–Al layered double hydroxide (LDH) was used as the support, which upon calcination in N<sub>2</sub>, dehydrated to the oxide form (LDO), effectively coating the gold nanoparticles. The LDO-induced SMSI improved the activity of the catalyst for ethanol dehydrogenation and CO oxidation while also inhibiting sintering. Interestingly, this technique was also employed to synthesize stable Rh/LDO and Pt/LDO with increased sintering resistance when calcined at 600 °C, indicating the universality of this approach.

Lee et al. published the first report on the use of the SMSI effect to stabilize a base metal catalyst against deactivation for APH of oxygenates. They reported both the geometric and bifunctional effects on titania-supported cobalt nanoparticles (Co/TiO<sub>2</sub>). The as-synthesized Co/TiO<sub>2</sub> catalyst was subjected to different thermal treatments and reduction conditions. A batch of the catalyst was reduced at 450 °C (Co/TiO<sub>2</sub> 723R) and 600 °C (Co/TiO<sub>2</sub> 873R), another batch

was calcined at 400 °C prior to reduction at 450 °C (Co/TiO $_2$  673C-723R) and 600 °C (Co/TiO $_2$  673C-873R), and the last batch was calcined at 600 °C and reduced at 600 °C (Co/TiO $_2$  873C-873R). Figure 11 shows a STEM image of the catalyst calcined at 600 °C, highlighting the SMSI protective layer over a Co nanoparticle.

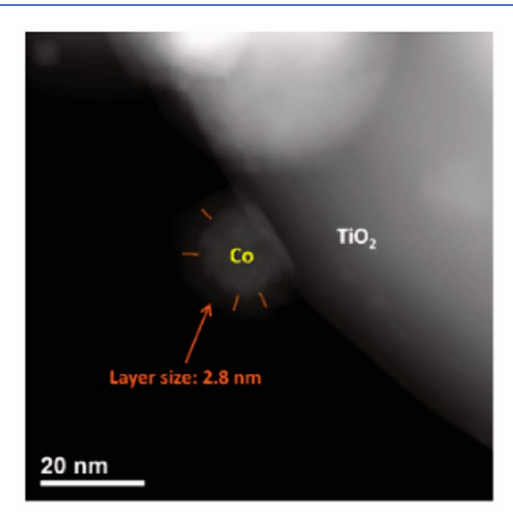


**Figure 11.** STEM image of Co/TiO<sub>2</sub> calcined at 600 °C. <sup>81</sup> Reproduced with permission from ref 81. Copyright 2015 Elsevier.

These catalysts were studied in the APH of furfuryl alcohol. ICP results showed no leaching for all catalysts reduced at 600 °C, while those reduced at 450 °C lost up to 44.6% of cobalt through leaching (Figure 12). Additionally, the carbon balance

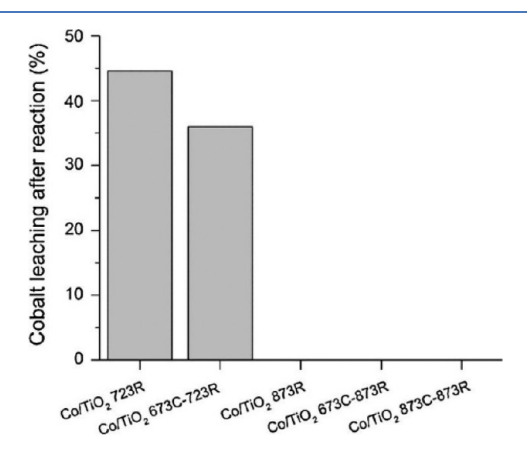


Figure 12. Cobalt leaching of the different  $Co/TiO_2$  catalysts after reaction. Reproduced with permission from ref 81. Copyright 2015 Elsevier.

for the catalyst reduced at 450 °C was lower than 69%, while that for the catalyst reduced at 600 °C was higher than 85%, which implied that catalysts reduced at 600 °C were more resistant to leaching and coking. The catalysts reduced at 600 °C also exhibited a higher selectivity to 1,2-pentanediol (30.3%), a product not observed when the catalyst was reduced at 450 °C. These results are indicative of the creation of bifunctional sites at high-temperature calcination and reduction, which facilitate the hydrogenolysis giving rise to high selectivity to 1,2-pentanediol.

Wang et al. also demonstrated that the SMSI effect was able to improve the stability of a Ni/MgO catalyst in the CO<sub>2</sub>

reforming of methane (CRM) reaction.<sup>82</sup> Calcination treatments led to the formation of a NiO-MgO solid solution as verified by XRD, in which all the NiO diffused and became incorporated into the MgO phase at calcination temperatures greater than 650 °C. Further reduction of this catalyst at 850 °C produced metallic Ni sites with improved activity and stability against sintering and reduced deposition of carbonaceous species. A similar approach was reported by Gonzalez-DelaCruz et al., who also discussed the stabilization of Ni/ CeO<sub>2</sub> via SMSI for the dry methane reforming.<sup>83</sup> In this work, they found that the Ni particles flattened and spread out on the partially reduced ceria surface. 83 This shape modification led to an improvement in the stability of the catalyst for dry reforming of methane at the typical high-temperature reaction conditions (750 °C). Later, in situ spectroscopy studies conducted by Caballero et al. confirmed that the SMSI effect in a Ni/CeO2 system led to the decoration and encapsulation of the Ni nanoparticles by the reduced ceria support.<sup>84</sup>

Another example of Ni catalysts with improved selectivity and stability was provided by Li et al., who synthesized a Ni@ ZrO<sub>2</sub> nanocomposite with enhanced metal-support interaction for hydrogen production from ethanol steam reforming.85 As Ni is prone to oxidation in air, NiO was used to synthesize the catalyst. NiO was first prepared via a surfactantassisted route, and the Ni@ZrO2 nanocomposite was synthesized via a modified hydrothermal method with the NiO particles added during the gelation of the zirconia precursor. A Ni/ZrO2 catalyst prepared by impregnation was also synthesized for comparison. As it can be seen on the TEM images in Figure 13c,d, the Ni@ZrO2 catalyst showed a higher dispersion than the Ni/ZrO2 catalyst, with an average Ni particle size of 10.5 nm compared with 23.7 nm. The presence of different zirconia crystalline phases is depicted in Figure 13a, being monoclinic zirconia  $(28.2^{\circ})$  and pure zirconia  $(31.5^{\circ})$ predominant on the Ni/ZrO2 catalyst. However, a metastable

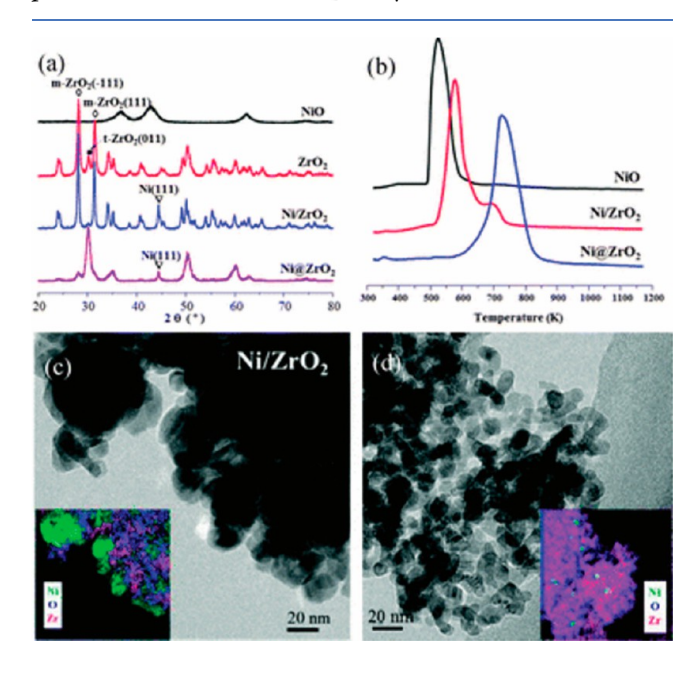


**Figure 13.** (a) XRD patterns recorded for NiO, ZrO<sub>2</sub>, Ni/ZrO<sub>2</sub>, and Ni@ZrO<sub>2</sub>, (b) TPR plots for NiO, Ni/ZrO<sub>2</sub>, and Ni@ZrO<sub>2</sub>, (c) TEM image and elemental mapping of Ni/ZrO<sub>2</sub>, and (d) TEM image and elemental mapping of Ni@ZrO<sub>2</sub>. <sup>85</sup> Reproduced with permission from ref 85. Copyright 2012 Royal Society of Chemistry.

Table 2. Reagents Employed for the Synthesis of Catalysts by the Stöber Method and Main Physical Properties

catalyst	metal source	reagents	reaction	$S_{BET} \choose m^2 \cdot g^{-1}$	particle size (nm)
Ni/SiO <sub>2</sub> <sup>97</sup>	$Ni(NO_3)_2 \cdot 6H_2O$	TEOS, C <sub>18</sub> TMS, NH <sub>3</sub> solution	methane decomposition	93-105	29-32
Ni/SiO <sub>2</sub> <sup>98</sup>	$Ni(NO_3)_2 \cdot 6H_2O$	TEOS, C <sub>18</sub> TMS, NH <sub>3</sub> solution	methane decomposition	93	32
Fe/SiO <sub>2</sub> <sup>98</sup>	$Fe(NO_3)_3 \cdot 9H_2O$	TEOS, C <sub>18</sub> TMS, NH <sub>3</sub> solution	methane decomposition	99	30
Co/SiO <sub>2</sub> <sup>98</sup>	$Co(NO_3)_2 \cdot 6H_2O$	TEOS, C <sub>18</sub> TMS, NH <sub>3</sub> solution	methane decomposition	50	50
NiO@SiO <sub>2</sub> <sup>99</sup>	Ni(acac) <sub>2</sub>	TMOS, C <sub>18</sub> TMS, NH <sub>3</sub> solution	methane reforming		46
NiO@SiO <sub>2</sub> <sup>91</sup>	$Ni(NO_3)_2 \cdot 6H_2O$	TEOS, PVP, NH <sub>3</sub> solution	syngas methanation	34-117	11.2-46.3
NiO@SiO <sub>2</sub> <sup>100</sup>	$Ni(NO_3)_2 \cdot 6H_2O$	TEOS, PVP, NH <sub>3</sub> solution	syngas methanation	263	11.2
Fe <sub>3</sub> O <sub>4</sub> @C/Ni <sup>101</sup>	$NH_4Fe(SO_4)_2 \cdot 12H_2O$	(NH <sub>4</sub> ) <sub>6</sub> Mo <sub>7</sub> O <sub>24</sub> ·4H <sub>2</sub> O, NaBH <sub>4</sub> , NH <sub>3</sub> solution	reduction of 4-nitrophenol	77	_
	NiCl <sub>2</sub> ·6H <sub>2</sub> O				
Ru@HCS <sup>22</sup>	RuCl <sub>3</sub>	TEOS, CTAB, NH <sub>3</sub> solution	Fischer-Tropsch	75	_
Ru@MHCS <sup>22</sup>	RuCl <sub>3</sub>	TEOS, CTAB, resorcinol, formaldehyde, $\mathrm{NH}_3$ solution	Fischer-Tropsch	944	_
Ru-Co@SiO <sub>2</sub> <sup>102</sup>	RuCl <sub>3</sub>	TEOS, PVP, NH <sub>3</sub> solution	methane reforming	55	52
	$Co(NO_3)_2 \cdot 6H_2O$				
Pd@SiO <sub>2</sub> <sup>103</sup>	PdCl <sub>2</sub>	TEOS, PVP, NH <sub>3</sub> solution	methane combustion	51-70	78-121
Pd@mSiO <sub>2</sub> <sup>103</sup>	PdCl <sub>2</sub>	TEOS, PVP, CTAB, NH <sub>3</sub> solution	methane combustion	610-764	78-91
PdPt@SiO <sub>2</sub> <sup>104</sup>	PdCl <sub>2</sub> , H <sub>2</sub> PtCl <sub>6</sub>	TEOS, PVP, CTAB, NH <sub>3</sub> solution	methane combustion	598	67
Au@MCM-22 <sup>105</sup>	$HAuCl_4$	TEOS, hexamethyleneimine, $Na_2Al_2O_4$ , $NH_3$ solution	oxidation of cyclohexane	392	_
Au@meso- SiO <sub>2</sub> 106	HAuCl <sub>4</sub>	TEOS, CTAB, F127, resorcinol, formaldehyde, $\mathrm{NH}_3$ solution	reduction of 4-nitrophenol	537	_

phase of zirconia at 30.3° was observed on Ni@ZrO2, which indicates a form of interaction with the nickel species. Likewise, the temperature-programmed reduction (TPR) profile (Figure 13 b) for Ni/ZrO2 showed a peak at 579 K with a shoulder at 693 K, while that for Ni@ZrO2 only showed a peak centered at 723 K. The higher reduction temperature confirmed the presence of NiOx species with strong interaction with the ZrO2 support. The geometric confinement of the Ni nanoparticles by zirconia coupled with the strong interaction between the components led to increased resistance of the nickel particles to sintering. In addition, the presence of surface-active oxygen enabled the removal of carbon deposits, thereby preventing coking on the catalyst. This catalyst proved to be stable for over 50 h on stream.

The SMSI effect applied to metals from the platinum group is still an area under much investigation. Fewer reports have shown the encapsulation of base metals using this technique. An important advantage of the SMSI effect is the enhancement of the catalytic activity and tunability to selective reactions and products. The modification of the activity by the adsorbate-mediated pathway and the versatility of its application to different supports calls for more explorative works and insights. Further, more focus should be geared toward developing the wet chemistry SMSI approach and applying it especially to non-noble metals.

Another interesting strategy gaining attention is the use of smart (or intelligent) catalysts, described as catalysts consisting of metal nanoparticles supported on perovskite-type materials. Akin to the SMSI effect, this technique leverages interactions between metal nanoparticles and the support as a result of reductive-oxidative treatments. This high affinity results in the solubilization of the metal cation into the support during calcination treatments preventing the sintering of the nanoparticles, which can then be exposed back to the surface upon reduction. For example, Nishihata et al. reported the self-regeneration of Pd-perovskites catalysts (La-Fe<sub>0.57</sub>Co<sub>0.38</sub>Pd<sub>0.05</sub>O<sub>3</sub> and LaFe<sub>0.95</sub>Pd<sub>0.05</sub>O<sub>3</sub>) for control of automotive emissions. <sup>86</sup> The catalysts were prepared via the alkoxide method, in which metal ethoxyethylates,

 $M^{3+}(OC_2H_4OC_2H_5)_3$  (M= La, Fe, and Co) are dissolved in toluene, and the precipitates containing Pd are obtained by using a diluted aqueous solution of Pd(NO<sub>3</sub>)<sub>2</sub> during hydrolysis. After drying, these were calcined to obtain the uniformly dispersed Pd-perovskites. They observed that upon exposure to oxidative (800 °C in air) and reductive atmospheres (800 °C in 10%  $H_2/90\%$   $N_2$ ), the Pd particles move inside and outside of the perovskite structure, respectively, inhibiting their growth and retaining its high catalytic activity during aging experiments. Conversely, a traditional impregnated Pd/alumina catalyst lost 10% of its activity when exposed to the same aging treatment. In related studies, Onn et al. reported the use of ALD to prepare a smart Pd catalyst on high-surface-area LaFeO<sub>3</sub>.87 Using ALD, these authors were able to deposit a thin conformal coating of LaFeO<sub>3</sub> on porous MgAl<sub>2</sub>O<sub>4</sub> for increased surface area. This allowed for an improved form of the self-regenerating smart catalyst compared with traditional bulk perovskite supports. This invariably opened new pathways for exploring ALD mechanisms for the incorporation of metal nanoparticles on perovskite supports for enhanced activity and stability. The use of non-noble metals for the development of smart catalysts has also been investigated. As an example, Deng et al. synthesized a smart Ni catalyst supported on LaFeO3 perovskite for the oxidative reforming of methane.<sup>88</sup> They observed that the cyclical embedment and redispersion of Ni enhanced its sintering and coking resistance during the reaction. They also studied the effect of different promoters (Pr, Mg, Sr, Ba, Ca, Ce) on the reducibility of Ni and concluded that Pr provided the greatest enhancement on the reduction of  $Ni^{3+}$  and eased the reversible diffusion of Ni atoms outside and inside the surface of the perovskite matrix (self-regeneration).

#### 5. STÖBER METHOD

The Stöber method was reported in 1968 as a sol—gel method to synthesize silica spheres with controlled diameter and uniform particle size. <sup>89</sup> It is a common method that takes place in a water—alcohol-ammonia-tetraalkoxysilane system, in which the spherical silica nanoparticles are formed via

ammonia-catalyzed hydrolysis and condensation of tetraethyl orthosilicate (TEOS) in alcohol-water mixtures. The Stöber method is also a well-established route to coat nanomaterials with a silica shell, and it has been widely employed in the encapsulation of metal<sup>90</sup> and metal oxide nanoparticles,<sup>91</sup> semiconductors,<sup>92</sup> polymers,<sup>93</sup> energy storage,<sup>94</sup> biotechnology,<sup>95</sup> and photonic devices.<sup>96</sup> As sintering and leaching are the main irreversible causes of catalyst deactivation, the Stöber method has been recently considered as a promising alternative to reduce these deactivation modes, and its efficiency has been evaluated in different catalytic active phases. Table 2 compiles some examples of catalysts synthesized by the Stöber process or derived methods, indicating the primary reagents used in the synthetic procedure and their main physical properties. These examples represent two different approaches: coprecipitation (e.g., Ni/SiO<sub>2</sub>) and core-shell (e.g., NiO@SiO<sub>2</sub>, with NiO: core and SiO<sub>2</sub>: shell). While the coprecipitation route involves the simultaneous nucleation and growth of metal and metal oxide, in the core-shell approach, the metallic core is synthesized first followed by deposition of the outer protective shell.

Wang et al. synthesized a series of NiO@SiO2 core-shell catalysts by using a modified Stöber method and studied them in the methanation of syngas.<sup>91</sup> These catalysts displayed a uniform encapsulation by SiO<sub>2</sub>, mutual coherence of the shells, and increased thickness upon the increase of the particle size. They found that the catalytic performance considerably decreased when increasing the calcination temperature during preparation, likely due to an increase of the NiO nanoparticle size. Unfortunately, the deactivation of the catalyst took place despite the formation of core-shell structures. However, a positive effect was detected on the core-shell catalysts prepared by the Stöber method when compared to a NiO-SiO<sub>2</sub> catalyst prepared by physical mixture, as the latter showed very low activity. Ashik et al. employed a continuous process denominated coprecipitation cum modified Stöber method, which avoided the use of high calcination temperature before coating nanoparticles with silica, reducing their agglomeration. 97 In this case, the SiO<sub>2</sub> protective layer around NiOH particles was synthesized through hydrolysis of TEOS and octadecyltrimethoxysilane (C<sub>18</sub>TMS) with ammonia in an alcoholic medium. Then, the catalyst was calcined and treated in H<sub>2</sub> to reduce NiO. The nanostructured n-Ni/SiO<sub>2</sub> catalyst prepared by this method displayed better catalytic stability than traditional Ni/SiO<sub>2</sub> catalysts for the hydrogen production by decomposition of methane, maintaining its catalytic activity for 300 min of time on stream with slight deactivation. In contrast, uncoated Ni nanoparticles suffered sintering and coking, with a thick layer of carbon hindering the further decomposition of methane over NiO. This research group also compared Ni/SiO<sub>2</sub>, Fe/SiO<sub>2</sub>, and Co/SiO<sub>2</sub> catalysts prepared by coprecipitation cum modified Stöber method for the thermocatalytic decomposition of methane.<sup>98</sup> They reported that the catalytic behavior, in terms of activity and stability, followed the order: Ni/SiO<sub>2</sub> > Co/SiO<sub>2</sub> > Fe/SiO<sub>2</sub>. The formation of large metal particles and metal particle fragmentation were responsible for the worse catalytic performance of Co/SiO<sub>2</sub> and Fe/SiO<sub>2</sub> catalysts, as the crystal size promoted the formation of irregularly shaped nanocarbons as a byproduct, which inhibited the catalytic activity. A more extensive study was carried out with the n-Ni/SiO2 catalyst through methane decomposition kinetic experiments in a fixed bed pilot plant.<sup>107</sup> Despite this catalyst being the most active,

the deactivation occurred under certain reaction conditions, such as high temperature and lower CH<sub>4</sub> partial pressure, due to carbon accumulation.

Yang et al. synthesized a Ni@SiO<sub>2</sub> core—shell catalyst by the Stöber approach and used the method of etching with hydrochloric acid to obtain a Ni@SiO<sub>2</sub> yolk—shell catalyst (Figure 14). 99 Although both core—shell and yolk—shell

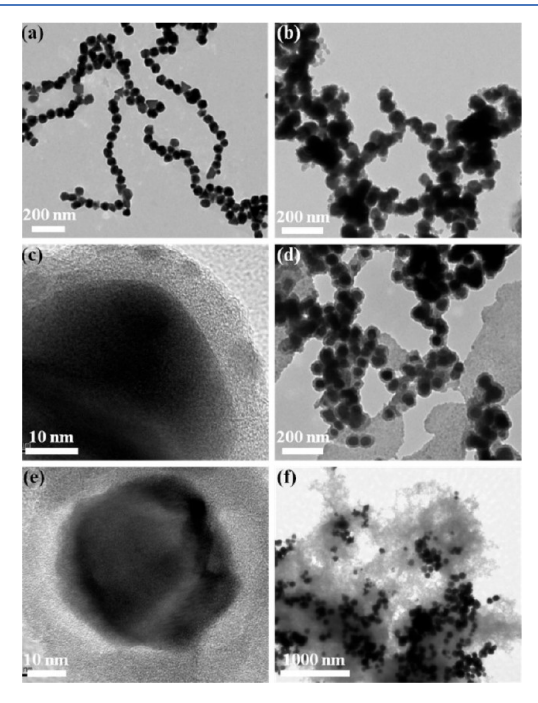


**Figure 14.** (a) TEM image of Ni nanoparticles, (b) TEM and (c) HRTEM images of Ni@SiO<sub>2</sub> core—shell catalyst, (d) TEM and (e) HRTEM images of Ni@SiO<sub>2</sub> yolk—shell catalyst, and (f) TEM image of Ni-SiO<sub>2</sub>-AE catalyst. P Reproduced with permission from ref 99. Copyright 2016 Elsevier.

structures are composed of Ni cores embedded in a silica shell, in the yolk-shell nanoarchitecture exists a void space between the metallic core and the oxide shell, thus creating individual nanoreactors around the core nanoparticles. The assynthesized catalyst was studied in the CO<sub>2</sub> reforming of CH<sub>4</sub> to syngas, and its behavior was compared with another Ni-SiO<sub>2</sub> catalyst prepared by a similar method but without full encapsulation of Ni particles by silica (Ni-SiO<sub>2</sub>-AE). It was reported that the sintering of the nickel particles was considerably decreased on the yolk-shell structured Ni@ SiO<sub>2</sub> catalyst, with enhanced stability of the material at a temperature up to 800 °C. Moreover, almost no encapsulating carbon was detected for this catalyst, which could be due to the gradual growth of filamentous carbon. However, the Ni@SiO<sub>2</sub> core-shell catalyst displayed less stability under the same conditions due to the deposition of encapsulating carbon that blocked the pores of the SiO<sub>2</sub> shell preventing the accessibility of the reactants to the active sites. In the case of the nonfully encapsulated Ni-SiO<sub>2</sub>-AE catalyst, both sintering of the Ni nanoparticles and carbon deposition were prevalent, with high carbon content up to 49% between encapsulating and filamentous carbon recorded after only 1.5 h on stream. Although the yolk-shell architecture displayed much better stability, there is usually a reduced metal-oxide interaction when this strategy is utilized because of the isolation of the metal cores inside the oxide shells. 108

Likewise, Han et al. also prepared core—shell structured Ni@SiO $_2$  catalysts by using chemical precipitation of NiO nanoparticles followed by a modified Stöber method for the syngas methanation reaction. Here, the stability of Ni@SiO $_2$  was higher than that of a traditional Ni/SiO $_2$  catalyst due to the strong interaction between the Ni core and the SiO $_2$  shell, which minimized the sintering of Ni particles and the carbon deposition. Moreover, the core—shell structured Ni@SiO $_2$  catalyst showed better textural properties (i.e., higher surface area and larger pore size), likely due to the blockage of the silica pores by NiO nanoparticles in the case of the Ni/SiO $_2$  catalyst.

A highly active catalyst comprised of NiO-MgO nanoparticles was also coated with silica using the Stöber protocol for increased stability by Li et al.  $^{109}$  The metal oxide nanoparticles were synthesized using a surfactant-assisted coprecipitation method, after which the oxides were encapsulated with porous silica. The as-prepared catalyst was utilized for the  $\rm CO_2$  methanation reaction. The authors reported that the catalyst with a Ni/Mg ratio of 4 exhibited the highest catalytic activity and stability for 100 h on stream at 300  $^{\circ}\rm C$ . This was attributed to the highly dispersed and isolated Ni nanoparticles because of the confinement effect of the silica shell protecting the particles from sintering.

In addition to Ni nanoparticles, the Stöber method has been employed to study other metal and metal oxide phases. For example, Wang et al. carried out the synthesis of Fe<sub>3</sub>O<sub>4</sub>@C/Ni microtubes and evaluated their catalytic behavior in the reduction of 4-nitrophenol. 101 First, a layer of nickel ion-doped polydopamine (PDA-Ni<sup>2+</sup>) was polymerized in situ on the surface of MoO3@FeOOH by an extended Stöber method using MoO3 as the sacrificing template in such a way that the PDA-Ni<sup>2+</sup> coating and the removal of MoO<sub>3</sub> were carried out simultaneously, facilitating the synthesis procedure. The prepared FeOOH@PDA-Ni<sup>2+</sup> microtubes were converted to Fe<sub>3</sub>O<sub>4</sub>@C/Ni through pyrolysis in an inert atmosphere without any additional reductants, leading into a material with large pore volume and BET surface area. This catalyst showed an excellent catalytic performance toward the reduction of 4-nitrophenol and interesting cyclic stability. On the other hand, Ai et al. synthesized a novel egg-like nanosphere by using a modified Stöber method with template-free surface-protected etching, Fe<sub>3</sub>O<sub>4</sub>@nSiO<sub>2</sub>-NH<sub>2</sub>-Fe<sub>2</sub>O<sub>3</sub>·xBi<sub>2</sub>O<sub>3</sub>@mSiO<sub>2</sub> (Figure 15), and evaluated its catalytic performance in the reduction of nitroaromatics to aniline. 110 First, a magnetic inner-core of Fe<sub>3</sub>O<sub>4</sub> spheres denominated as "yolk" was covered by a layer of nonporous silica in which amino groups were introduced by using 3aminopropyl-triethoxysilane (APTES). The Fe-based nanoparticles were magnetically immobilized around these magnetic silica spheres bonded to the surface of amino groups; this inner silica shell bearing active Fe<sub>2</sub>O<sub>3</sub>·xBi<sub>2</sub>O<sub>3</sub> species named as "egg white." Finally, this material was protected by using polyvinylpyrrolidone and then etched with NaOH to increase the permeability of the outer silica shell, being denominated as the "egg-shell," and calcinated at 350 °C. This novel mesoporous-silica-protected egg-like nanocatalyst demonstrated to be an efficient and chemoselective catalyst for the reduction of several functionalized nitroarenes to their corresponding anilines. Thus, high values of catalytic activity and selectivity and long lifetimes were found in such a way that the presence of Bi enhanced the activity of iron oxide, and the

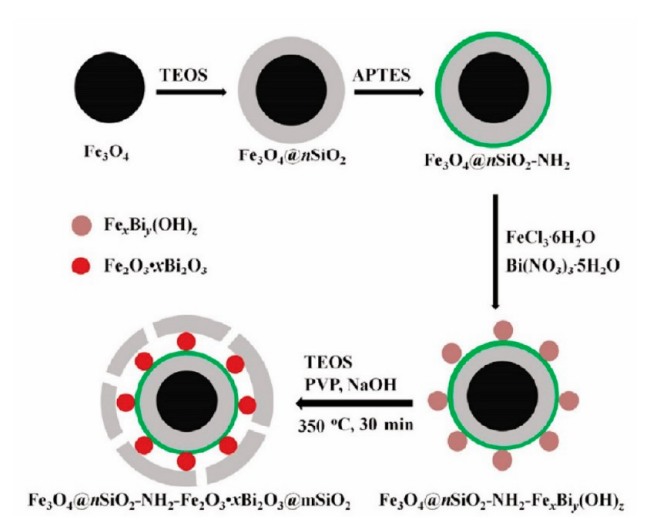


**Figure 15.** Synthesis schematic for Fe<sub>3</sub>O<sub>4</sub>@nSiO<sub>2</sub>-NH<sub>2</sub>-Fe<sub>2</sub>O<sub>3</sub>· xBi<sub>2</sub>O<sub>3</sub>@mSiO<sub>2</sub> core—shell catalyst. <sup>110</sup> Reproduced with permission from ref 110. Copyright 2017 Springer Nature.

active component  $Fe_2O_3\cdot xBi_2O_3$  reduced the aggregation of the active phase.

Another example of encapsulation by a modified Stöber process was reported by Pang et al., who synthesized bimetallic Ru–Co catalysts for the CO<sub>2</sub> reforming of methane to syngas. They reported that the encapsulation of nanoparticles with silica enhanced their thermal stability due to particle isolation and contributed to reducing sintering and suppressed cobalt oxidation during the reaction. Overcoated Ru–Co catalysts with uniform Ru distribution and optimum porosity of the SiO<sub>2</sub> shell demonstrated to be highly stable and efficient at low temperatures. Likewise, these authors evaluated the effect of adding surfactants, polyvinylpyrrolidone (PVP) and cetyltrimethylammonium bromide (CTAB), to the shell to improve its porosity, and they found that this was critical for mass transportation and catalytic activity.

The coating of cobalt particles has been reported to be challenging due to the poor stability and magnetic properties of metallic cobalt particles in solution. 111 Kobayashi et al. reported the first case of a Co@SiO2 core-shell structure when they synthesized amorphous Co nanoparticles encapsulated with a dense homogeneous silica shell. 112 The same technique was utilized to overcoat large Co nanoparticles by Wu et al.; 113 however, there were some challenges related to the dispersion of the cobalt nanoparticles and mass transfer limitations due to the lack of homogeneity of the overcoating layer. Batail et al. also reported the encapsulation of cobalt nanoparticles in mesoporous silica using a modified Stöber synthesis with a high surface area and improved stability in oxidation conditions. 114 In this work, the cobalt nanoparticles were stabilized using sodium nitrate and polyvinylpyrrolidone (PVP). The as-synthesized cobalt nanoparticles were then coated using a modified Stöber protocol. They focused on optimizing the amount of solid per pass and the induced porosity in the silica shell without causing a significant effect on the metallic properties. To achieve this, the authors utilized a pseudomorphic transformation of the Co@m-SiO2 material in an alkaline solution of CTAB and subjected the prepared catalyst to annealing conditions in an atmosphere of air. In situ XRD and TEM analyses revealed that the cobalt catalyst was

very resistant to oxidation and stable against sintering even up to 700  $^{\circ}\text{C}.$ 

The Stöber method has also been used to protect gold catalysts from deactivation. As an example, Arnal et al. prepared  $Au@ZrO_2$  catalysts by covering Au nanoparticles with a dense silica layer by a modified Stöber process, coating this with a zirconia shell, and subsequently removing the  $SiO_2$  core (Figure 16).<sup>115</sup> The isolation of the metal nanoparticles

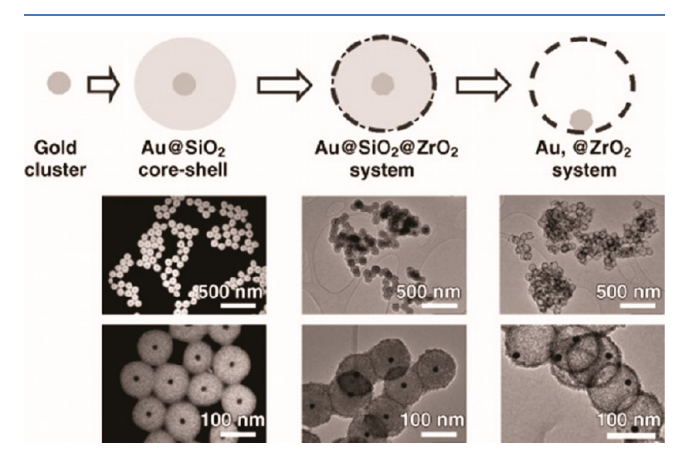


**Figure 16.** Schematic and TEM images of the Au@SiO<sub>2</sub> core—shell, Au@SiO<sub>2</sub>@ZrO<sub>2</sub>, and Au@ZrO<sub>2</sub> catalysts. Reproduced with permission from ref 115. Copyright 2006 John Wiley and Sons.

by the hollow sphere encapsulation allowed the stabilization of the active phase for CO oxidation, unlike the nonencapsulated catalyst, which suffered a considerable loss of catalytic activity. Coated and uncoated Au catalysts were both subjected to thermal treatment at 800 °C, and it was observed that the particle size of the coated particles was unchanged, while the uncoated catalyst suffered from sintering. The uncoated catalyst also suffered a significant drop-off in the activity for the CO oxidation reaction after calcination at 800 °C corroborating the sintering effect, while the coated catalyst maintained its activity even after calcination.

Similarly, Saxena et al. also encapsulated Au nanoparticles with silica by the Stöber method and further transformed this into Au@ZSM-5 and Au@MCM-22 by a modified hydrothermal route. 105 The Au nanoparticles encapsulated by zeolite nanoshells displayed better catalytic performance for the cyclohexane oxidation reaction (a reaction driven by acid sites) than commercial and conventional zeolites, improving their sintering resistance, decreasing the agglomeration, and enhancing the conversion. Several other authors also studied the encapsulation of Au nanoparticles by the Stöber method for the reduction of 4-nitrophenol. Chen et al. synthesized mesoporous silica hollow nanospheres with multiple Au cores (Figure 17). 106 First, core-shell Au@resorcinol-formaldehyde nanospheres with multiple gold cores were synthesized by a modified Stöber method. Then, the core-shell nanospheres were coated with a layer of mesoporous silica by using CTAB as a template, giving rise to Au@meso-SiO2 after calcination. This catalyst displayed high catalytic activity and stability for the reduction of 4-nitrophenol.

Likewise, Fang et al. developed novel Au-loaded magnetic SiO<sub>2</sub>/carbon yolk–shell ellipsoids (Fe@SiO<sub>2</sub>–Au@H–C), which were composed of magnetic Fe@SiO<sub>2</sub> yolks, mesoporous carbon shells, and multiple gold nanoparticles. <sup>116</sup> For this, the SiO<sub>2</sub>/polymer resin double-shell structures were first

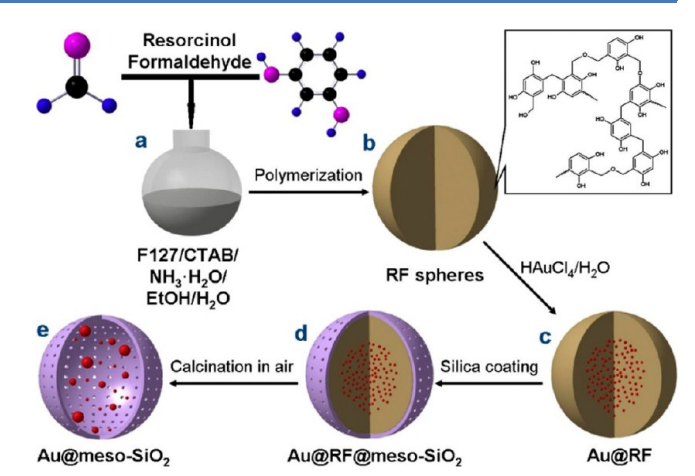


**Figure 17.** Synthesis protocol for Au@meso-SiO<sub>2</sub> catalyst. <sup>106</sup> Reproduced with permission from ref 106. Copyright 2014 Elsevier.

prepared by an extended Stöber method, followed by carbonization-hydrothermal etching to obtain yolk-shell structures with mesoporous carbon shells. Finally, the in situ encapsulation of Au nanoparticles and the integration of inner entrapped Fe cores with strong magnetism were simultaneously accomplished via H<sub>2</sub> reduction. The gold nanoparticles showed good dispersion and enhanced thermal stability because of the protection of ethylenediamine as a stabilizer. This catalyst demonstrated to be active for the reduction of 4nitrophenol and easily recoverable for its reuse. Recently, Yang et al. encapsulated Au nanoparticles inside hollow mesoporous carbon spheres that were synthesized from biopolymeric chitosan via an in situ Stöber approach followed by pyrolysis and alkali washing. These yolk-shell architectures (YS-Au@ HMCS) showed larger catalytic activity and stability than others for the reduction of 4-nitrophenol because of decreased deactivation through leaching of the active phase. 117

Other noble metal core—shell structures have also been developed using the Stöber method. Palladium core—shell structures prepared by the Stöber synthesis were shown to operate effectively at temperatures much lower than the commercial conditions for the hydrogenation of 4-carboxylbenzaldehyde (4-CBA) to p-toluic acid. This hydrogenation process is the primary upgrading step in the refining of purified terephthalic acid (PTA), and lower operating temperature and effective isolation of the palladium particles by the porous silica shell was shown to mitigate possible challenges associated to sintering of the Pd particles in the PTA refining process.

Joo et al. also reported the synthesis of platinum/ mesoporous silica core-shell catalysts (Pt@mSiO<sub>2</sub>). 119 These catalytic structures demonstrated high thermal stability for high-temperature CO oxidation reaction studies, including ignition behavior, which was not possible with bare Pt owing to the metal aggregation. The platinum core in Pt@mSiO<sub>2</sub> maintained its morphology and crystalline nature up to 750 °C. Interestingly this Pt core-shell catalysts also exhibited good activity for the ethylene hydrogenation reaction. Shang et al. also reported the encapsulation of graphene-supported Pt nanoparticles using mesoporous silica. 12 In this case, the hydrolysis of TEOS was initiated by ammonium hydroxide derived from the decomposition of urea, forming a mesoporous silica shell over the catalyst. CTAB was used to generate pores on the silica overlayer, after which the catalyst

Table 3. Reagents Employed on the Synthesis of Mixed Oxides by Nonhydrolytic Sol-Gel Method and Main Physical Properties

mixed oxides	metal source	reagents	reaction	$S_{\rm BET}~({\rm m}^2\cdot{\rm g}^{-1})$
Co-Al <sup>132</sup>	CoCl <sub>2</sub> , AlCl <sub>3</sub>	diisopropyl ether	epoxidation of $(Z)$ -cyclooctene	45
Jacobsen-Al <sup>133</sup>	Jacobsen, AlCl <sub>3</sub>	diisopropyl ether	oxidation of $(Z)$ -cyclooctene	31
Re-Al <sup>134</sup>	ReCl <sub>5</sub> , AlCl <sub>3</sub>	diisopropyl ether	metathesis of ethene and butene	360
Re-Si-Al <sup>134</sup>	ReCl <sub>5</sub> , SiCl <sub>4</sub> , AlCl <sub>3</sub>	diisopropyl ether	metathesis of ethene and butene	190
Si-Ti <sup>127</sup>	$Si(OAc)_4$ , $Ti(NEt_2)_4$	Pluronic P123	epoxidation of cyclohexene	442
TiO <sub>2</sub> @SBA-15 <sup>135</sup>	TiCl <sub>4</sub> , Ti(OiPr) <sub>4</sub>	diethyl ether	1-phenylethanol dehydration	292-350
Ni/Si-Ti <sup>136</sup>	SiCl <sub>4</sub> , TiCl <sub>4</sub> , Ni(NO <sub>3</sub> ) <sub>2</sub> ·6H <sub>2</sub> O	diisopropyl ether	ethane dehydrogenation	83-156
$V-Ti^{137}$	VOCl <sub>3</sub> , TiCl <sub>4</sub>	diisopropyl ether	oxidation of benzene	64-88
$W-V-Ti^{138}$	WCl <sub>6</sub> , VOCl <sub>3</sub> , TiCl <sub>4</sub>	diisopropyl ether	oxidation of benzene	58-109
$Mo-V-Ti^{138}$	MoCl <sub>5</sub> , VOCl <sub>3</sub> , TiCl <sub>4</sub>	diisopropyl ether	oxidation of benzene	53-90
$W-Zr-Si^{139}$	WCl <sub>6</sub> , ZrCl <sub>4</sub> , SiCl <sub>4</sub>	diisopropyl ether	dehydration of glycerol	79–635

was annealed in hydrogen to reduce the graphene oxide support. This catalyst showed superior stability than the uncoated catalyst and remained stable up to 700 °C in Ar. The catalyst also displayed better activity in the APH of 4-nitrophenol (4-NP) to 4-aminophenol (4-AMP) and retained its activity after four cycles.

Habibi et al. studied in depth the accessibility to metal sites in SiO<sub>2</sub>-encapsulated Pd catalysts (Pd@SiO<sub>2</sub>) and compared several synthetic routes to modify the porosity of the shell while maintaining a Pd nanoparticle size of 8 nm. 103 Although the encapsulation of Pd nanoparticles protected the metal cores from sintering, the use of PVP alone was not advisable as the resulting structure was practically nonporous Pd@SiO<sub>21</sub> exhibiting low catalytic activity for methane combustion due to the inaccessibility of Pd sites. As in the case reported by Shang et al., the incorporation of an additional porogen, such as CTAB, to the Stöber synthetic procedure (Pd@mSiO<sub>2</sub>) enhanced the shell porosity without losing Pd, reaching full conversion in the CH4 combustion reaction under similar conditions than the traditional impregnated catalysts but with improved stability. These authors also encapsulated bimetallic Pd-Pt nanoparticles in silica shells using a Stöber-based method, which employed both PVP and CTAB. 104 These catalysts provided higher values of conversion for methane combustion than other impregnated PdPt/Al<sub>2</sub>O<sub>3</sub> and PdPt/ SiO<sub>2</sub> catalysts because of the higher metal dispersion provided by the shells and enhanced stability, remaining unchanged for 70 h of time on stream.

Therefore, the encapsulation by the Stöber method should be considered as a promising alternative to prevent leaching or sintering of metal nanoparticles for heterogeneous catalytic processes.

#### 6. NONHYDROLYTIC SOL-GEL METHOD

It is well-known that sol—gel chemistry, which is based on hydrolysis and condensation of molecular precursors, such as metal alkoxides, is a powerful technique for the synthesis of catalytic metal oxides. However, this method possesses several disadvantages, mainly the disparity in the hydrolysis reaction rates, which provokes the loss of microstructural control over final oxides and the collapse of the pore network due to drying by evaporation. Description 222,123 One attractive alternative is the use of nonaqueous conditions by using oxygen donors other than water, which is known as nonhydrolytic sol—gel (NHSG) chemistry. Thus, NHSG methods involve different condensation reactions and nonaqueous media that affect the stoichiometry, homogeneity, and textural properties of multi-

component oxides, being particularly useful for the synthesis of metal oxide nanoparticles. For example, NHSG methods could be used to overcome the challenges associated with the use of mesoporous oxides at a larger scale, such as leaching of the active phase, and the relatively low mechanical and hydrothermal stability. Even when there are many examples of mixed oxides prepared by NHSG in the literature, most of them were not synthesized with the purpose of controlling the catalyst deactivation. Lisa, 123, 126–131 In this section, we will only discuss examples focused on reducing the deactivation processes.

De Lima et al. prepared a cobalt complex entrapped in alumina by a nonhydrolytic sol—gel route to catalyze the epoxidation of (Z)-cyclooctene using iodozylbenzene as the oxygen donor. This hybrid material was obtained through condensation of aluminum chloride with diisopropylether in the presence of cobalt chloride (Table 3). Unlike the Co—Al catalysts prepared by a conventional hydrolytic sol—gel method, no cobalt leaching was detected for samples synthesized by the NHSG method. Jacobsen's catalyst, a compound of manganese and a salen-type ligand shown in Figure 18, has also been entrapped in alumina by a nonhydrolytic sol—gel route for its use in the oxidation of (Z)-cyclooctene, styrene, and cyclohexene by using different oxidants. Here, a solution of AlCl<sub>3</sub> and diisopropyl ether was

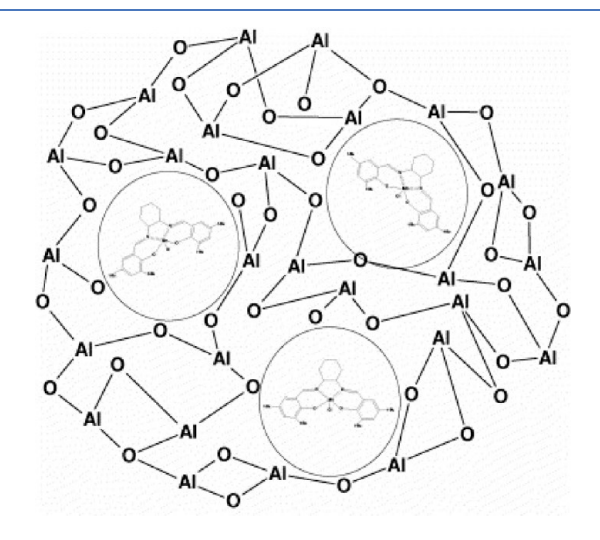


**Figure 18.** Schematic view of Jacobsen catalyst in an alumina matrix. <sup>133</sup> Reproduced with permission from ref 133. Copyright 2006 Elsevier.

Figure 19. Sol—gel NHSG based on condensation reaction between metallic (or silicon) halides and metallic (or silicon) alkoxides. <sup>140</sup> Reproduced with permission from ref 140. Copyright 2010 Elsevier.

heated in the presence of the salen complex, forming an alumina gel containing the Mn(salen)complex in its skeleton that remained entrapped after alumina precipitation. The aging step was key to consolidate the structure by condensation and bond formation. In addition to better yields, this catalyst could also be reused for several cycles without apparent leaching of the active phase, in contrast to catalysts prepared by conventional hydrolytic sol—gel processes. It was concluded that the use of the NHSG method prevented the chemical degradation of the Mn(salen) and increased the stability of the material.

Ricci et al. also synthesized novel alumina catalysts containing Fe(III) ions by the NHSG route for their use in the oxidation of hydrocarbons, such as cyclooctene and cyclohexane. This synthetic procedure was based on an alkyl halide elimination via etherolysis/condensation between AlCl<sub>3</sub> and diisopropyl ether in the presence of FeCl<sub>3</sub>, followed by treatment of the obtained xerogel at different temperatures (Figure 19). Fe(III) ions were firmly incorporated onto the alumina matrix after thermal treatment at temperatures higher than 400 °C, as leaching of the active phase was not detected under these synthetic conditions, demonstrating that the thermal treatment was a key factor for the stability of the active phase of the catalysts.

Another example was provided by Bouchmella et al., who developed different Re-based mixed oxides (Re-Si, Re-Al and Re-Si-Al) by a NHSG route followed by calcination and evaluated their catalytic performance in the cross-metathesis of ethene and butene to propene. 134 It has been previously reported that losses of rhenium frequently occur during calcination due to sublimation. 141 This fact was suppressed on Re-Al and Re-Si-Al catalysts with alumina-rich formulations as Re species migrated toward the surface and became highly dispersed without loss of Re during the calcination step. The Re-Si-Al catalysts were more active than Re-Al and Re-Si, being the latter inactive, and their catalytic deactivation was lower than that observed for Mo-based catalysts under the same reaction conditions. Later, the same research group carried out the synthesis of rhenium oxide-based catalysts with various Re<sub>2</sub>O<sub>7</sub> loadings and SiO<sub>2</sub>/Al<sub>2</sub>O<sub>3</sub> ratios by using a NHSG method for olefin metathesis. 142 They demonstrated that Re sublimation did not happen during the calcination step even at high rhenium loadings, attaining highly active mixed oxide catalysts for the metathesis of olefins.

On the other hand, different TiO<sub>2</sub>-SiO<sub>2</sub> catalysts prepared by NHSG method have been reported in the literature. Skoda

et al. synthesized mesoporous titanosilicate xerogels based on the condensation between silicon tetraacetate (Si(OAc)<sub>4</sub>) and titanium(IV) diethylamide (Ti(NEt<sub>2</sub>)<sub>4</sub>) to obtain Ti-O-Si linkages for their use in cyclohexene epoxidation. 127 They observed that the addition of Pluronic P123 as a structuredirecting agent enhanced the porosity of the materials and dispersed tetrahedral Ti species. They also reported that the pore network collapsed upon heating of xerogels without a template, breaking Ti-O-Si bonds and forming small TiO<sub>2</sub> crystallites. Additionally, the use of P123 contributed to preserving the Ti-O-Si bonds and the active fourcoordinated Ti sites during heating, avoiding leaching of the Ti species. Therefore, these stable mesoporous Si-Ti catalysts exhibited high catalytic efficiency for conversion of cyclohexene to cyclohexene oxide achieving a yield of 96%. Smeets et al. also prepared mesoporous SiO2-TiO2 catalysts by a NHSG route modified to increase the surface hydrophobicity, as catalysts were deactivated in the presence of water during the catalytic conversion of cyclohexene with  $H_2O_2$ . 143 Postgrafting methylation allowed for an excellent combination of a hydrophobic surface with a high content of active sites, which led to high epoxidation activity while protecting the active sites from the inactivating effect of water.

Héroguel et al. synthesized TiO2 overcoats by using a NHSG method to encapsulate different metal oxide and metal catalysts for the 1-phenylethanol dehydration reaction and deoxygenation of lignin-derived propyl guaiacol. The TiO2 thin film deposition was carried out in a single liquid phase step involving the continuous injection of NHSG precursors, titanium tetrachloride (TiCl<sub>4</sub>) and titanium isopropoxide (Ti(O<sup>i</sup>Pr)<sub>4</sub>), giving rise to uniform coatings. The deposition was first realized on a model Cu<sub>2</sub>O and SiO<sub>2</sub> spheres. By using TEM together with EDX mapping, they were able to confirm the formation of conformal overcoats after TiO2 deposition (Figure 20). After that, they carried out the deposition of TiO<sub>2</sub> layers within the mesoporous structure of SBA-15 to generate medium-strength Lewis acid sites, which catalyzed the dehydration of 1-phenylethanol while limiting the catalyst deactivation. Therefore, NHSG overcoating enhanced the catalytic selectivity by controlling the metal oxide surface functionalities. Likewise, overcoating supported metal Pt nanoparticles (TiO<sub>2</sub>@Pt/SiO<sub>2</sub>) increased the selectivity of propylcyclohexane during the conversion of 3-propylguaiacol as the TiO<sub>2</sub> overcoat was able to suppress the catalyst deactivation through nanoparticle sintering.

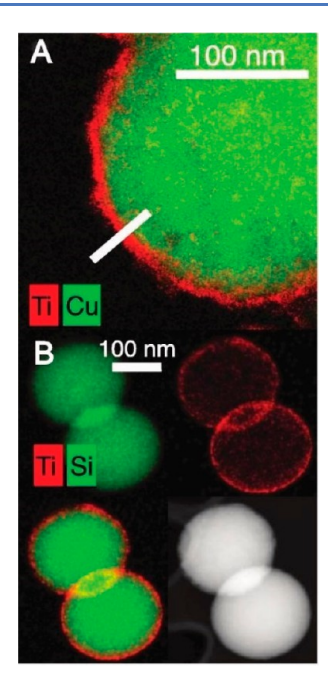


**Figure 20.** TEM images and corresponding EDX mapping for (a)  $30\text{TiO}_2$ @Cu<sub>2</sub>O (Cu: green; Ti: red) and (b)  $10\text{TiO}_2$ @SiO<sub>2</sub> (Si: green; Ti: red). <sup>135</sup> Reproduced with permission from ref 135. Copyright 2018 Elsevier.

Another example was provided by Debecker et al., who synthesized V2O5-TiO2 catalysts by NHSG routes for the oxidation of benzene. First, they prepared efficient catalysts based on V<sub>2</sub>O<sub>5</sub> and TiO<sub>2</sub> with controlled composition and texture from chloride precursors, where most of the V species migrated toward the surface of anatase nanoparticles. 137 These materials were active in the oxidation of benzene, and no catalyst deactivation was observed during the experiments, suggesting that oligomeric vanadates are more efficient than isolated VO<sub>x</sub> species. Later, they employed MoO<sub>3</sub> and WO<sub>3</sub> as promoters to increase the efficiency of V<sub>2</sub>O<sub>5</sub>/TiO<sub>2</sub> catalysts synthesized by the NHSG route. 138 At low and medium V<sub>2</sub>O<sub>5</sub> loadings, MoO<sub>3</sub> demonstrated to be a better promoter than WO<sub>3</sub> due to incomplete migration of W species; however, Mocontaining catalysts were less active than W-containing ones at high V<sub>2</sub>O<sub>5</sub> loadings because part of TiO<sub>2</sub> was found as rutile in the first case.

Studies with tungsten oxide-containing catalysts prepared by NHSG routes for control of catalyst deactivation have also been found in the literature. Oakton et al. synthesized several WO<sub>x</sub> materials via NHSG method by using different W precursors, WCl<sub>4</sub> and WCl<sub>6</sub>, in the presence of diisopropyl ether. 144 These catalysts showed lower deactivation than WO<sub>3</sub> in the photocatalytic oxygen evolution from water. Nadji et al. prepared mixed WO<sub>3</sub>-SiO<sub>2</sub> and WO<sub>3</sub>-ZrO<sub>2</sub>-SiO<sub>2</sub> catalysts by NHSG method for glycerol dehydration to acrolein. 139 All catalysts were active and selective to acrolein due to the high proportion of Brønsted acid sites, and the authors concluded that the one-pot nonhydrolytic sol-gel route was an effective synthetic method to obtain active, selective, and stable catalysts for the aerobic transformation of glycerol to acrolein. Finally, Ullmann et al. immobilized Cp2ZrCl2 on SiO2 by using two different methods: direct grafting and via entrapment within the silica matrix by a NHSG route, modifying the surface of the latter with various metal salts (Cr, Mo, and W). 145 They found that the NHSG approach allowed the incorporation of Lewis

acid sites while supporting the catalyst by entrapping in a single gelation step. It was suggested that the higher activities of these entrapped systems could be related to the Lewis acid sites on the surface, which prevented them from deactivation through poisoning.

Therefore, the nonhydrolytic sol—gel route seems to be an attractive approach not only for the synthesis of mixed oxide catalysts but also for control of catalyst deactivation through entrapping of the active sites.

# DEPOSITION AND GRAFTING OF ORGANIC COMPOUNDS IN LIQUID MEDIA

Other nonconventional encapsulation methods have been studied in the literature. Pham et al. reported the deposition of carbon layers onto the surface of different oxide supports to be used for liquid-phase reactions. 146 In this work, carbon was obtained from the pyrolysis of simple sugars (sucrose). Approximately 10 wt % of carbon was deposited to form a thin layer onto SBA-15 mesoporous silica, commercial silica gel, and commercial fumed alumina. For carbon deposition, an aqueous solution of sucrose was added to the desired support and stirred overnight at room temperature until water evaporation. Then, the dry sample was partially pyrolyzed under nitrogen flow at 300 °C for 2 h with a ramp rate of 5 °C· min<sup>-1</sup>. The samples were then subjected to hydrothermal treatment at 100 °C and 22 bar of autogenous pressure for 12 h. It was observed that SBA-15 became more hydrophobic after coating with carbon, making the surface more resistant to hydrophilic attack. Likewise, while the XRD patterns of the uncoated alumina samples showed the formation of boehmite species, the carbon-coated samples did not present them due to the presence of the carbonaceous layer. In addition, they also proved that a high dispersion of palladium particles was possible on these carbon-coated oxides, which opens additional pathways for novel catalyst designs.

In a similar work, Lin et al. reported the use of a hydrophobic carbon layer to overcoat a Ni/TiO $_2$  catalyst for its application in aqueous reaction media. <sup>147</sup> A hydrothermal synthesis protocol containing glucose as the carbon source was also used here. Different carbon loadings (2, 11, and 29.2 wt %) were deposited, and the success of the coating of the Ni/TiO $_2$  catalyst was confirmed by using different characterization techniques. TPR plots of the Ni/TiO $_2$  and carbon-coated Ni/TiO $_2$  catalysts are shown in Figure 21. The Ni/TiO $_2$  sample

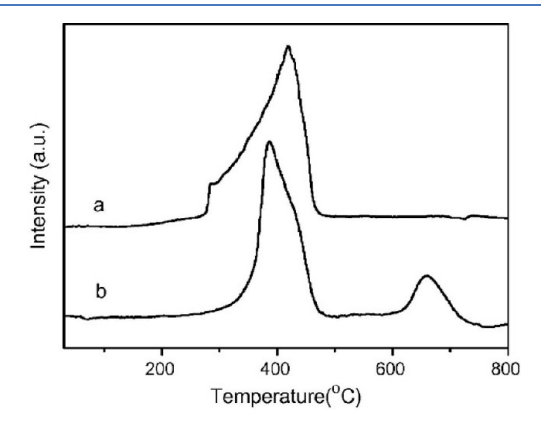


**Figure 21.** TPR profiles for (a) Ni/TiO<sub>2</sub> and (b) (Ni/TiO<sub>2</sub>)@C-11%.  $^{147}$  Reproduced with permission from ref 147. Copyright 2012 Elsevier.

showed one reduction peak centered at 419 °C, which was attributed to the interaction between NiO and TiO2, while the shoulder at 285 °C was assigned to bulk NiO with no interaction with the TiO<sub>2</sub> surface. On the other hand, the (Ni/ TiO<sub>2</sub>)@C-11% carbon-coated catalyst showed two reduction peaks at 386 and 660 °C. The first peak at 386 °C was assigned to the reduction of NiO, and the lower temperature indicated a more facile reduction of NiO through carbon modification. The second reduction peak at 660 °C was attributed to the reduction of the carbon-coated surface. The catalytic performance of coated and uncoated catalysts was evaluated in the hydrogenation of nitrobenzene in water. The activity studies showed that all coated catalysts showed better conversion than the uncoated catalyst, with the 11% C-coated catalyst exhibiting the highest reaction rate. The results suggested that the 2 wt % coated catalyst did not effectively encapsulate the catalyst while the 29.2 wt % coated catalyst created a thick coating layer leading to mass transfer limitations. Stability studies revealed that the 11% C-coated catalyst regained its conversion of ~98% after 3 runs, while the conversion of the uncoated catalyst dropped markedly from ~80 to <10%, indicating the deactivation of the catalyst. The loss of activity of the uncoated Ni/TiO<sub>2</sub> catalyst was attributed to chemical changes of the active species as the reaction progressed.

There have also been other reports in which metal oxide supports have been modified with organic groups to improve the catalyst resistance to deactivation. For example, Jenkins et al. recently reported the utilization of alkyl phosphonic-acid (PA) self-assembled monolayers (SAMs) to enhance the stability of Au/TiO<sub>2</sub> catalysts. Modified and unmodified catalysts were subjected to thermal treatment at 700 °C in air for 4 h, obtaining average particle sizes of 5.9 and 8.0 nm, respectively, indicating an increased resistance to sintering in the modified catalyst. Sintering of the particles was prevented entirely up to 450 °C, while the unmodified catalyst experienced a 47% increase in average particle size. The TEM images and particle size distribution of the thermally treated catalysts at 450 °C are shown in Figure 22. Reactivity

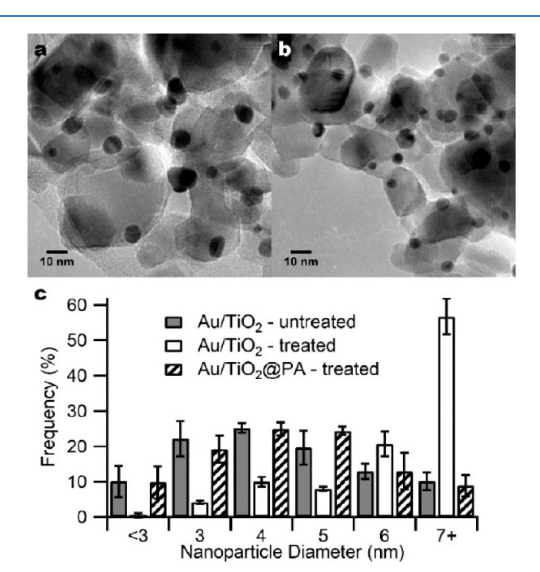


**Figure 22.** TEM image of thermally treated (a) unmodified and (b) PA-modified Au/TiO<sub>2</sub>, and (c) particle size distribution for Au/TiO<sub>2</sub>, thermally treated Au/TiO<sub>2</sub>, and thermally treated Au/TiO<sub>2</sub>@PA.<sup>148</sup> Reproduced with permission from ref 148. Copyright 2019 American Chemical Society.

studies showed that the PA-modified catalyst was well suited for reactions conducted at moderate temperatures under reduction conditions, such as the hydrogenation of acetylene, with significant prevention of sintering and coke formation.

Van den Berg et al. functionalized a silica support prepared by the Stöber method by treating it with aminopropyltriethoxysilane (APTES) to suppress the formation and/or transport of copper species and reduce the catalytic deactivation in the methanol synthesis reaction. This treatment led to the introduction of aminopropyl groups on the silica surface via the reaction between the APTES and the surface hydroxyl groups. Cu was then deposited on the functionalized support via incipient wetness impregnation, and the catalyst was used in the synthesis of methanol in a continuous fixed bed reactor. It was reported that the functionalization of the support with APTES increased the stability of the catalyst by favoring the dispersion of Cu due to stronger interaction between CuO and the support. It was also concluded that the silica functionalization retarded the Ostwald ripening phenomenon, which was the most probable particle growth mechanism.

#### 8. OTHER ENCAPSULATION METHODS

In addition to the methods previously described, there have been other strategies reported in the literature for the synthesis of core—shell architectures. One of the disadvantages of these structures is the limited accessibility to the active sites of the catalyst due to the thickness of the outer layer. Regardless, these methods have been widely used to control the deactivation through sintering and leaching.

Bakhmutsky et al. investigated the behavior of certain oxide shells (CeO<sub>2</sub>, TiO<sub>2</sub>, and ZrO<sub>2</sub>) over palladium and platinum cores and studied these catalysts in the water-gas shift (WGS) reaction. 151 The increased reducibility of the CeO<sub>2</sub> and TiO<sub>2</sub> shells akin to SMSI led to increased transient deactivation in both metal cores, an effect that was observed to be more pronounced on Pd cores, revealing that the interactions between the metals and the shells were significant. The ZrO<sub>2</sub> shell catalysts displayed the least transient deactivation owing to the less susceptibility of the ZrO2 shell to reduction. Similarly, Arroyo-Ramírez et al. compared Pt@CeO2/Si-Al<sub>2</sub>O<sub>3</sub> and Pd@CeO<sub>2</sub>/Si-Al<sub>2</sub>O<sub>3</sub> core-shell structures and observed that greater interaction between Pd and CeO<sub>2</sub> led to a more stabilized catalyst against sintering. <sup>152</sup> However, the encapsulation of Pd by reduced ceria resulted in a reduction of the activity for the WGS reaction. Furthermore, the Pt@ CeO<sub>2</sub>/Si-Al<sub>2</sub>O<sub>3</sub> catalyst was less stable, and the particles were sintered at high temperatures. These results are similar to those reported by Cargnello et al., in which the increased stability of Pd@CeO<sub>2</sub> came at the expense of reduced accessibility to the active sites. 153 Cargnello et al. were able to develop highly dispersible and tunable Pd@CeO2 core-shell nanostructures via a self-assembly pathway between functionalized Pd nanoparticles protected by 11-mercaptoundecanoic acid (MUA) and cerium(IV) alkoxide. 154 In related studies, these Pd@CeO2 nanostructures were deposited onto alumina and proved to be highly stable and active for the combustion of methane. 155 Microscopy studies revealed that the Pd@CeO<sub>2</sub> core-shell nanostructures remained intact even after calcination at 850 °C. Remarkably, the complete conversion was observed at 400 °C using this catalyst, which is 130 °C less than that required for the supported Pd/CeO<sub>2</sub> system. Adijanto et al. demonstrated that Pd@CeO2 core-shell

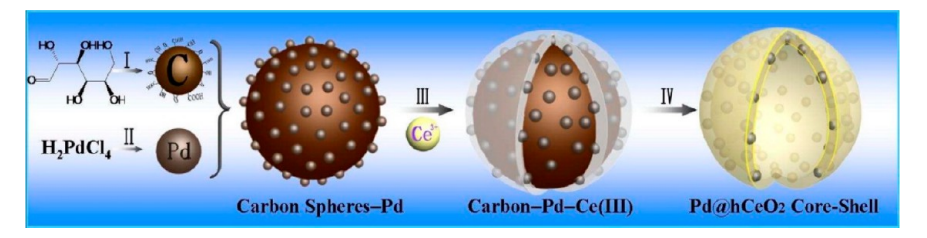


Figure 23. Schematic illustration of the synthesis of  $Pd@hCeO_2$  core—shell structures. Reproduced with permission from ref 157. Copyright 2013 American Chemistry Society.

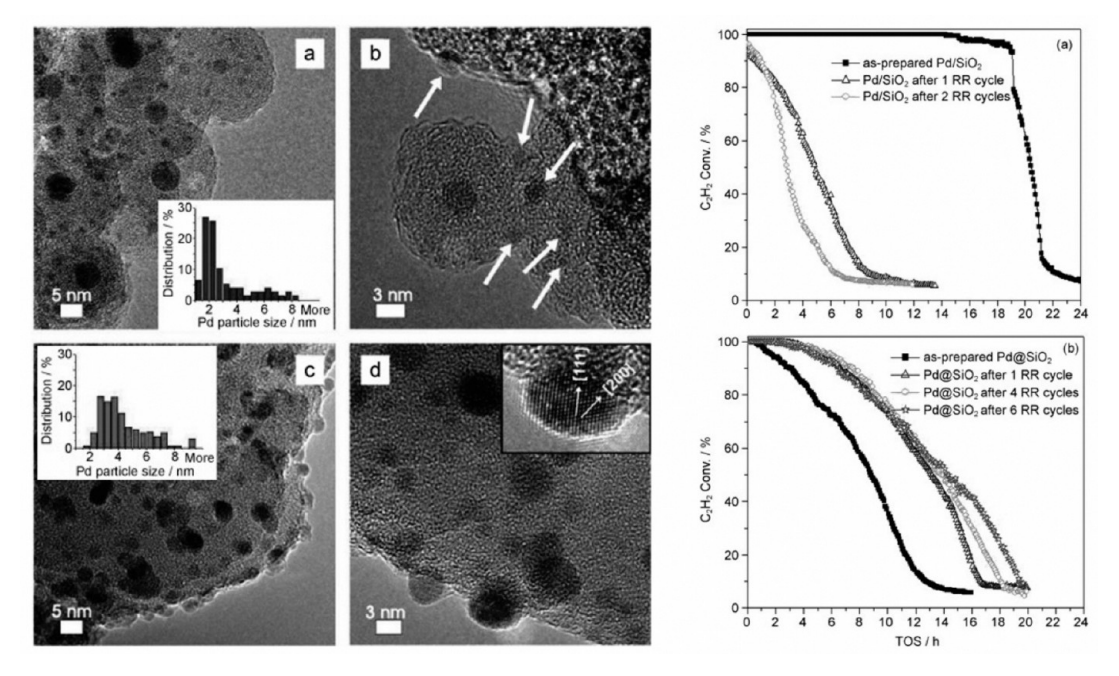


Figure 24. TEM images of as-synthesized  $Pd@SiO_2$  (top images) and  $Pd@SiO_2$  after 6 regeneration cycles in 50%  $O_2/Ar$  at 500 °C for 3 h (bottom images) and catalytic activity of  $Pd/SiO_2$  compared to  $Pd@SiO_2$  catalyst. Reproduced with permission from ref 158. Copyright 2010 John Wiley and Sons.

deposited on yttria-stabilized zirconia (YSZ) using alkyl coupling agents were highly resistant to sintering even up to 700 °C and exhibited high activity for the methane combustion reaction. 156

Zhang et al. utilized core-shell techniques to create a stable palladium metal catalyst. They reported the synthesis of a Pd@ hCeO2 catalyst composed of palladium nanoparticles encapsulated inside of cerium oxide hollow shells (Figure 23). 157 First, carbon spheres, which served as a template, were fabricated by hydrothermal treatment of an aqueous solution of glucose. Then, PVP-capped Pd nanoparticles were synthesized via an alcohol reductive process by dissolving PdCl2 in an aqueous solution of HCl to form a H<sub>2</sub>PdCl<sub>4</sub> solution, which was then mixed with water, ethanol, and PVP and maintained under reflux at 90 °C for 3 h. To obtain the encapsulated material, Pd colloids were added to a dispersed solution of the assynthesized carbon spheres followed by addition of a CeCl<sub>3</sub> aqueous solution, and the mixture was stirred for 20 min before subjecting it to hydrothermal treatment (180 °C, 6 h) in an autoclave reactor. After hydrothermal treatment, the sample was recovered, dried, and calcined in air at 500 °C to remove the carbon spheres, leading to the formation of coreshell particles with hollow inner space. This strategy was effective in preventing both sintering and leaching with

excellent reusability properties in the selective reduction of aromatic nitro compounds in water under ambient conditions.

Forman et al. followed a water-in-oil microemulsion method to prepare silica-coated palladium cores (Pd@SiO2), and the stability of this catalyst against sintering and coking was studied in the hydrogenation of acetylene. 158 When compared with a catalyst synthesized by deposition of Pd nanoparticles onto silica (Pd/SiO<sub>2</sub>), the encapsulated catalyst showed much slower deactivation and could be easily regenerated (Figure 24). While the acetylene conversion was significantly reduced on the Pd/SiO<sub>2</sub> catalyst after one reaction-regeneration cycle, the Pd@SiO2 core-shell catalyst displayed an increased activity after one cycle, and it maintained its activity through five successive cycles. Interestingly, the authors concluded that the silica encapsulation was able to suppress not only coking but also the in situ formation of palladium carbide. 158 A similar water-in-oil microemulsion strategy was reported for the stabilization of Fe on silica with an improved activity for CO hydrogenation. 159 Park et al. also made use of a microemulsion approach to encapsulate Pd with silica using TEOS as the silica precursor and *n*-octadecyltrimethoxysilane to increase the shell porosity. 160 The core-shell Pd@SiO<sub>2</sub> catalyst was thermally stable up to 700 °C in air, and it also showed improved stability for the oxidation of CO and hydrogenation of acetylene when compared to a conventional supported catalyst.

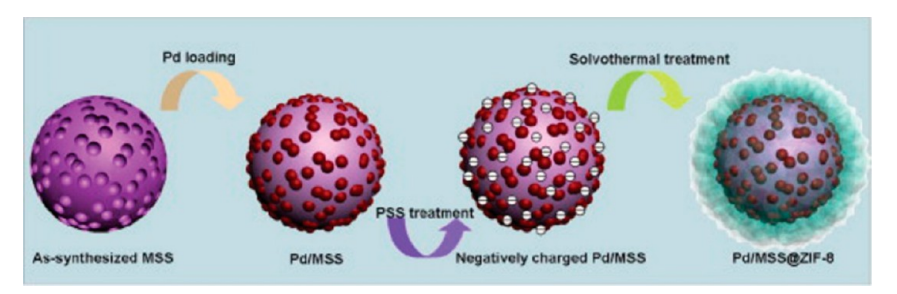


Figure 25. Schematic of the synthesis of the Pd/MSS@ZIF-8 composite. 162 Reproduced with permission from ref 162. Copyright 2014 Elsevier.

Furthermore, Ying et al. used a reverse micelle method to encapsulate palladium cores with a silica shell (Pd@SiO $_2$ -RM). Using this technique, they were able to prepare ultrasmall Pd nanoparticles ( $\sim$ 1.1 nm) in a one-pot synthesis. The reverse micelle encapsulated nanoparticles exhibited a higher metal surface area when compared with others encapsulated by the Stöber method and regular microemulsion processes, as well as the traditional impregnation catalysts. Consequentially, the reverse micelle encapsulated catalyst exhibited superior activity and thermal stability in the oxidation of CO. As a result of the silica coating, the growth of palladium crystallites was effectively hindered up to calcination temperatures of 800 °C. Remarkably, the catalyst also demonstrated resistance toward deactivation by water vapor.

In a novel approach, Zhang et al. encapsulated a Pd catalyst with zeolitic imidazolate frameworks, ZIF-8, which is a class of metal—organic frameworks. The schematic process is shown in Figure 25. First, they synthesized Pd-decorated mesoporous silica spheres (Pd/MSS) by ion-exchange using Pd(NH<sub>3</sub>)<sub>4</sub>Cl<sub>2</sub>, followed by surface modification with a polyelectrolyte to facilitate the nucleation and growth of the ZIF-8 shell. <sup>162</sup> The catalytic activity of the encapsulated Pd/MSS@ZIF-8 catalyst was evaluated in the hydrogenation of 1-hexene and cyclohexene, and it was observed that the core—shell architecture prevented the leaching of the metal nanoparticles during the reaction, maintaining its catalytic activity. This material presented multiple advantages, such as excellent reactant shape-selectivity, antipoisoning capability, and good recyclability when compared with a conventional Pd/MSS catalyst.

Different core-shell structures have also been investigated to protect Au catalysts from deactivation. Yu et al. described the high thermal stability of a Au@SnO2 catalyst prepared by a facile intermetallics-based dry-oxidation method, which allowed for easy control of the core—shell size and also induced synergistic effects for the oxidation of CO. 163 Another approach was reported by Chen et al., who used a colloidal method to synthesize nanostructures with Au core and porous titania shell that were later deposited on hydrophobic alumina. 164 The Au@TiO2 core-shell catalyst was found to be stable against sintering up to 600 °C because of the improved metal-support interaction. Cargnello et al. showed that ceria could also be used to encapsulate gold cores (Au@ CeO<sub>2</sub>). Here, the presence of carboxylic groups over the gold nanoparticles was instrumental in directing the ceria shell formation. The Au@CeO2 catalyst was highly active for preferential oxidation of CO and did not exhibit any irreversible deactivation.

As the majority of these core—shell structures have been implemented for noble metal systems, more studies need to focus on the encapsulation of non-noble metals that are readily

available and less expensive. In addition, as challenges such as activity loss and diffusivity are important when using these approaches, more care and attention should be directed toward developing highly active and stable core—shell catalysts.

Another strategy reported in the literature for control of catalyst deactivation consists in the embedment of metal nanoparticles in the channels of mesoporous silica (Figure 26). A simple one-step synthetic method for insertion of

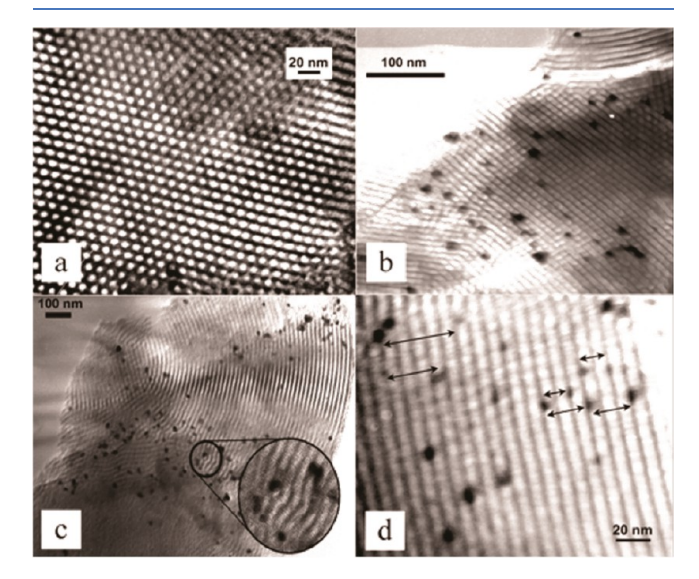


**Figure 26.** TEM images of Au nanoparticles encapsulated on the pores of SBA-15. <sup>166</sup> Reprinted with permission from ref 166. Copyright 2003 American Chemical Society.

metal oxide nanocrystals within the pores of SBA-15 was described by Yang et al.  $^{167}$  The process involved the hydrolysis of TEOS in the presence of metal precursors and a templating agent (Pluronic 123). Reddy et al. used this method to entrap cobalt species within the SBA-15 structure. 168 The synthesis was conducted via a precipitation process involving cobaltous chloride and TEOS. While a 2 wt % Co/SBA-15 embedded catalyst showed to be stable and exhibited 9.4% conversion in the oxidation of cyclohexane and 78% selectivity to cyclohexanone, a similar catalyst prepared via impregnation showed negligible catalytic activity. Another example was provided by Martínez et al., who synthesized an iron-containing SBA-15 catalyst. 169 The catalyst was prepared via co-condensation of FeCl<sub>2</sub> and TEOS under acidic conditions using Pluronic 123, resulting in crystalline Fe<sub>2</sub>O<sub>3</sub> particles within the channels of SBA-15. This catalyst proved to be highly active in the photo-Fenton degradation of phenolic aqueous solutions and stable toward leaching even at high hydrogen peroxide concentrations.

#### 9. CONCLUSIONS AND OUTLOOK

In this Review, we summarized different encapsulation techniques used to control the deactivation of heterogeneous catalysts and provided insights into the improvement of stability and activity when using encapsulated catalysts. In order to give the reader a better sense of understanding and knowledge of the developments in this field, the encapsulation techniques were classified primarily into CVD, ALD, SMSI, Stöber method, and NHSG methods. Other novel core—shell strategies and encapsulation/embedment methods were also discussed.

In some instances, there is a trade-off between activity and stability, such as in CVD. Certain techniques like ALD holds promising prospects because of the very thin conformal layers deposited; however, the cost associated with the large-scale implementation of this technology still remains a challenge. Although ALD has successfully been commercialized in the microelectronics industry, industrial application in catalysis synthesis would depend on the overall adoption of this technique in the catalyst market. Novel liquid-phase ALD techniques hold great potential due to the scale-up ability and the use of inexpensive precursors, which bodes well for the industrial implementation of this method. An interesting prospect would be to leverage on this technique to coat group VIII metal with SMSI-inducing oxides, such as TiO2 and ZrO2, as this could provide an avenue for tuning catalyst activity and selectivity for relevant reactions of interest. SMSI has been mostly used to create bifunctionality at the interface of metal-metal oxides systems, establishing new pathways for improving the activity; however, this phenomenon is only mostly observed with group 8B metals. Further studies on the wet chemistry SMSI technique could also provide more facile means to combat catalyst deactivation. Continual efforts should be geared toward inducing beneficial metal-support interaction via less energy intensive conditions compared to conventional high temperature reductive-oxidative pathways. The use of smart catalysts is also a very interesting area for study. Even when the use of ALD to prepare high-surface-area perovskite supports is already exciting, the utilization of ALD to synthesize well-tailored metal nanoparticles on high-surfacearea perovskite supports deserves exploration as this could open new routes for more precise control and fine-tuning of catalysts, along with optimization of the metal-support interactions for enhanced stability and activity. In parallel studies, the liquid-phase ALD technique could also be investigated to this end, as this could also facilitate industrial implementation of smart catalysts.

Some mass transfer limitations are still prevalent in these processes, such as in core—shell structures and the Stöber synthesis. The difficulty of controlling the shell thickness and porosity in these architectures are still areas of concern. As scientists develop more catalytic technologies for encapsulation, it would be convenient to leverage on other existing processes, such as sol—gel synthesis and colloidal methods, which are also economically viable. Efforts should be geared toward optimizing these processes and applying these techniques to develop more stable and active heterogeneous catalysts. In addition, further mechanistic studies on the growth of overlayers might direct future research efforts. The recent use of sugars to coat metal oxide supports with carbon also shows promise, mostly for reactions in aqueous media, such as those in biomass conversion. Future work should focus

on enhancing the stability of those carbon-coated oxides as catalytic supports to be used in aqueous-phase reactions.

In conclusion, it can be said that much progress has been made over the years, and this Review is meant to act as a guide to the catalyst community to leverage upon. Therefore, the information contained herein should inspire future explorative and collaborative works in improving catalyst stability and activity. It is the ultimate goal that this will foster innovative solutions for renewable and sustainable energy systems.

#### AUTHOR INFORMATION

#### **Corresponding Authors**

Ana C. Alba-Rubio — Department of Chemical Engineering, The University of Toledo, Toledo, Ohio 43606, United States; orcid.org/0000-0002-1831-8338; Email: ana.albarubio@utoledo.edu

Cristina García-Sancho — Departamento de Química Inorgánica, Cristalografia y Mineralogía, Facultad de Ciencias, Universidad de Málaga, 29071 Málaga, Spain; o orcid.org/ 0000-0003-4464-0432; Email: cristinags@uma.es

#### **Authors**

 Hope O. Otor – Department of Chemical Engineering, The University of Toledo, Toledo, Ohio 43606, United States
 Joshua B. Steiner – Department of Chemical Engineering, The University of Toledo, Toledo, Ohio 43606, United States

Complete contact information is available at: https://pubs.acs.org/10.1021/acscatal.0c01569

#### Notes

The authors declare no competing financial interest.

#### ACKNOWLEDGMENTS

This material is based upon work supported by the National Science Foundation under Grant No. 1847391. C.G.S. acknowledges support from FEDER (European Union) funds (UMA18-FEDERJA-171) and the University of Malaga. Authors are also thankful to I. G. Alba Rubio for the design of the graphical abstract and cover art.

### REFERENCES

- (1) Bartholomew, C. H. Mechanisms of catalyst deactivation. *Appl. Catal., A* **2001**, *212*, 17–60.
- (2) Goodman, E. D.; Schwalbe, J. A.; Cargnello, M. Mechanistic Understanding and the Rational Design of Sinter-Resistant Heterogeneous Catalysts. *ACS Catal.* **2017**, *7* (10), 7156–7173.
- (3) Argyle, M.; Bartholomew, C. Heterogeneous Catalyst Deactivation and Regeneration: A Review. *Catalysts* **2015**, *5* (1), 145–269.
- (4) Forzatti, P.; Lietti, L. Catalyst deactivation. *Catal. Today* **1999**, 52 (2-3), 165-181.
- (5) Moulijn, J. A.; Van Diepen, A. E.; Kapteijn, F. Catalyst deactivation: is it predictable? What to do? *Appl. Catal., A* **2001**, *212* (1–2), 3–16.
- (6) Hansen, T. W.; Delariva, A. T.; Challa, S. R.; Datye, A. k. Sintering of Catalytic Nanoparticles: Particle Migration or Ostwald Ripening. *Acc. Chem. Res.* **2013**, *46* (8), 1720–1730.
- (7) Besson, M.; Gallezot, P. Deactivation of metal catalysts in liquid phase organic reactions. *Catal. Today* **2003**, *81* (4), 547–559.
- (8) Neyestanaki, A. K.; Klingstedt, F.; Salmi, T.; Murzin, D. Y. Deactivation of postcombustion catalysts, a review. *Fuel* **2004**, *83* (4–5), 395–408.
- (9) Lange, J. P. Renewable Feedstocks: The Problem of Catalyst Deactivation and its Mitigation. *Angew. Chem., Int. Ed.* **2015**, *54* (45), 13186–13197.

- (10) Héroguel, F.; Rozmyslowicz, B.; Luterbacher, J. S. Improving Heterogeneous Catalyst Stability for Liquid-phase Biomass Conversion and Reforming. *Chimia* **2015**, *69* (10), 582–591.
- (11) Singh, J. A.; Yang, N.; Bent, S. F. Nanoengineering Heterogeneous Catalysts by Atomic Layer Deposition. *Annu. Rev. Chem. Biomol. Eng.* **2017**, *8*, 41–62.
- (12) Pan, C.-J.; Tsai, M.-C.; Su, W.-N.; Rick, J.; Akalework, N. G.; Agegnehu, A. K.; Cheng, S.-Y.; Hwang, B.-J. Tuning/exploiting Strong Metal-Support Interaction (SMSI) in Heterogeneous Catalysis. *J. Taiwan Inst. Chem. Eng.* **2017**, *74*, 154–186.
- (13) Sun, Y.; Wu, Q.; Shi, G. Graphene based new energy materials. *Energy Environ. Sci.* **2011**, *4* (4), 1113.
- (14) Singh, R.; Sansare, S.; Shidhaye, S. Biomedical application of graphenes. *Biomedical Applications of Nanoparticles* **2019**, 319–339.
- (15) Zhang, Y.; Zhang, L.; Zhou, C. Review of Chemical Vapor Deposition of Graphene and Related Applications. *Acc. Chem. Res.* **2013**, *46* (10), 2329–2339.
- (16) Obraztsov, A. N. Making graphene on a large scale. *Nat. Nanotechnol.* **2009**, *4*, 212–213.
- (17) Mattevi, C.; Kim, H.; Chhowalla, M. A review of chemical vapour deposition of graphene on copper. *J. Mater. Chem.* **2011**, *21* (10), 3324–3334.
- (18) Terranova, M. L.; Sessa, V.; Rossi, M. The World of Carbon Nanotubes: An Overview of CVD Growth Methodologies. *Chem. Vap. Deposition* **2006**, *12* (6), 315–325.
- (19) Cai, Z.; Liu, B.; Zou, X.; Cheng, H. M. Chemical Vapor Deposition Growth and Applications of Two-Dimensional Materials and Their Heterostructures. *Chem. Rev.* **2018**, *118* (13), 6091–6133.
- (20) Seipenbusch, M.; Binder, A. Structural Stabilization of Metal Nanoparticles by Chemical Vapor Deposition-Applied Silica Coatings. *J. Phys. Chem. C* **2009**, *113* (48), 20606–20610.
- (21) Xiong, H.; Schwartz, T. J.; Andersen, N. I.; Dumesic, J. A.; Datye, A. K. Graphitic-Carbon Layers on Oxides: Toward Stable Heterogeneous Catalysts for Biomass Conversion Reactions. *Angew. Chem., Int. Ed.* **2015**, *54* (27), 7939–7943.
- (22) Phaahlamohlaka, T. N.; Kumi, D. O.; Dlamini, M. W.; Jewell, L. L.; Coville, N. J. Ruthenium nanoparticles encapsulated inside porous hollow carbon spheres: A novel catalyst for Fischer—Tropsch synthesis. *Catal. Today* **2016**, *275*, 76–83.
- (23) Zhang, P.; Qiao, Z.-A.; Dai, S. Recent advances in carbon nanospheres: synthetic routes and applications. *Chem. Commun.* **2015**, *51* (45), 9246–9256.
- (24) Liu, C.; Wang, C.-C.; Kei, C.-C.; Hsueh, Y.-C.; Perng, T.-P. Atomic Layer Deposition of Platinum Nanoparticles on Carbon Nanotubes for Application in Proton-Exchange Membrane Fuel Cells. *Small* **2009**, *5* (13), 1535–1538.
- (25) Knez, M.; Nielsch, K.; Niinistö, L. Synthesis and Surface Engineering of Complex Nanostructures by Atomic Layer Deposition. *Adv. Mater.* **2007**, 19 (21), 3425–3438.
- (26) Pickrahn, K. L.; Gorlin, Y.; Seitz, L. C.; Garg, A.; Nordlund, D.; Jaramillo, T. F.; Bent, S. F. Applications of ALD MnO to electrochemical water splitting. *Phys. Chem. Chem. Phys.* **2015**, *17* (21), 14003–14011.
- (27) Kilbury, O. J.; Barrett, K. S.; Fu, X.; Yin, J.; Dinair, D. S.; Gump, C. J.; Weimer, A. W.; King, D. M. Atomic layer deposition of solid lubricating coatings on particles. *Powder Technol.* **2012**, *221*, 26–35.
- (28) Li, J.; Liang, X.; King, D. M.; Jiang, Y.-B.; Weimer, A. W. Highly dispersed Pt nanoparticle catalyst prepared by atomic layer deposition. *Appl. Catal., B* **2010**, 97 (1), 220–226.
- (29) Lu, J.; Elam, J. W.; Stair, P. C. Synthesis and Stabilization of Supported Metal Catalysts by Atomic Layer Deposition. *Acc. Chem. Res.* **2013**, *46* (8), 1806–1815.
- (30) Lu, J.; Elam, J. W.; Stair, P. C. Atomic layer deposition—Sequential self-limiting surface reactions for advanced catalyst "bottom-up" synthesis. *Surf. Sci. Rep.* **2016**, 71 (2), 410–472.
- (31) Pagan-Torres, Y. J.; Lu, J.; Nikolla, E.; Alba-Rubio, A. C. Well-Defined Nanostructures for Catalysis by Atomic Layer Deposition. In Morphological, Compositional, and shape control of materials for

- catalysis; Fornasiero, P., Cargnello, M., Eds.; Elsevier, 2017; pp 643-676.
- (32) Leskela, M.; Ritala, M. Atomic layer deposition (ALD): from precursors to thin film structures. *Thin Solid Films* **2002**, 409 (1), 138–146.
- (33) O'Neill, B. J.; Jackson, D. H. K.; Lee, J.; Canlas, C.; Stair, P. C.; Marshall, C. L.; Elam, J. W.; Kuech, T. F.; Dumesic, J. A.; Huber, G. W. Catalyst Design with Atomic Layer Deposition. *ACS Catal.* **2015**, 5 (3), 1804–1825.
- (34) Puurunen, R. L. Surface chemistry of atomic layer deposition: A case study for the trimethylaluminum/water process. *J. Appl. Phys.* **2005**, *97* (12), 121301.
- (35) Leskelä, M.; Ritala, M. Atomic layer deposition (ALD): from precursors to thin film structures. *Thin Solid Films* **2002**, 409 (1), 138–146.
- (36) Yan, H.; Cheng, H.; Yi, H.; Lin, Y.; Yao, T.; Wang, C.; Li, J.; Wei, S.; Lu, J. Single-Atom Pd1/Graphene Catalyst Achieved by Atomic Layer Deposition: Remarkable Performance in Selective Hydrogenation of 1,3-Butadiene. *J. Am. Chem. Soc.* **2015**, *137* (33), 10484–10487.
- (37) Ma, Z.; Brown, S.; Howe, J. Y.; Overbury, S. H.; Dai, S. Surface Modification of Au/TiO2 Catalysts by SiO2 via Atomic Layer Deposition. *J. Phys. Chem. C* **2008**, *112* (25), 9448–9457.
- (38) De Rogatis, L.; Cargnello, M.; Gombac, V.; Lorenzut, B.; Montini, T.; Fornasiero, P. Embedded phases: a way to active and stable catalysts. *ChemSusChem* **2010**, 3 (1), 24–42.
- (39) Biener, M. M.; Biener, J.; Wichmann, A.; Wittstock, A.; Baumann, T. F.; Bäumer, M.; Hamza, A. V. ALD Functionalized Nanoporous Gold: Thermal Stability, Mechanical Properties, and Catalytic Activity. *Nano Lett.* **2011**, *11* (8), 3085–3090.
- (40) Feng, H.; Lu, J.; Stair, P. C.; Elam, J. W. Alumina Over-coating on Pd Nanoparticle Catalysts by Atomic Layer Deposition: Enhanced Stability and Reactivity. *Catal. Lett.* **2011**, *141* (4), 512–517.
- (41) Feng, H.; Elam, J. W.; Libera, J. A.; Setthapun, W.; Stair, P. C. Palladium Catalysts Synthesized by Atomic Layer Deposition for Methanol Decomposition. *Chem. Mater.* **2010**, 22 (10), 3133–3142.
- (42) Lu, J.; Fu, B.; Kung, M. C.; Xiao, G.; Elam, J. W.; Kung, H. H.; Stair, P. C. Coking- and Sintering-Resistant Palladium Catalysts Achieved Through Atomic Layer Deposition. *Science* **2012**, 335 (6073), 1205–1208.
- (43) Onn, T. M.; Zhang, S.; Arroyo-Ramirez, L.; Chung, Y.-C.; Graham, G. W.; Pan, X.; Gorte, R. J. Improved Thermal Stability and Methane-Oxidation Activity of Pd/Al2O3 Catalysts by Atomic Layer Deposition of ZrO2. ACS Catal. 2015, 5 (10), 5696–5701.
- (44) O'Neill, B. J.; Jackson, D. H. K.; Crisci, A. J.; Farberow, C. A.; Shi, F.; Alba-Rubio, A. C.; Lu, J.; Dietrich, P. J.; Gu, X.; Marshall, C. L.; Stair, P. C.; Elam, J. W.; Miller, J. T.; Ribeiro, F. H.; Voyles, P. M.; Greeley, J.; Mavrikakis, M.; Scott, S. L.; Kuech, T. F.; Dumesic, J. A. Stabilization of Copper Catalysts for Liquid-Phase Reactions by Atomic Layer Deposition. *Angew. Chem., Int. Ed.* **2013**, *52* (51), 13808–13812.
- (45) O'Neill, B. J.; Sener, C.; Jackson, D. H. K.; Kuech, T. F.; Dumesic, J. A. Control of Thickness and Chemical Properties of Atomic Layer Deposition Overcoats for Stabilizing  $Cu/\gamma$ -Al2O3 Catalysts. *ChemSusChem* **2014**, 7 (12), 3247–3251.
- (46) Zhang, H.; Lei, Y.; Kropf, A. J.; Zhang, G.; Elam, J. W.; Miller, J. T.; Sollberger, F.; Ribeiro, F.; Akatay, M. C.; Stach, E. A.; Dumesic, J. A.; Marshall, C. L. Enhancing the stability of copper chromite catalysts for the selective hydrogenation of furfural using ALD overcoating. *J. Catal.* **2014**, *317*, 284–292.
- (47) Zhang, H.; Canlas, C.; Jeremy Kropf, A.; Elam, J. W.; Dumesic, J. A.; Marshall, C. L. Enhancing the stability of copper chromite catalysts for the selective hydrogenation of furfural with ALD overcoating (II) Comparison between TiO2 and Al2O3 overcoatings. *J. Catal.* **2015**, 326, 172–181.
- (48) Correa, G. C.; Bao, B.; Strandwitz, N. C. Chemical Stability of Titania and Alumina Thin Films Formed by Atomic Layer Deposition. ACS Appl. Mater. Interfaces 2015, 7 (27), 14816–14821.

- (49) Lee, J.; Jackson, D. H. K.; Li, T.; Winans, R. E.; Dumesic, J. A.; Kuech, T. F.; Huber, G. W. Enhanced stability of cobalt catalysts by atomic layer deposition for aqueous-phase reactions. *Energy Environ. Sci.* **2014**, *7* (5), 1657–1660.
- (50) Sundberg, P.; Karppinen, M. Organic and inorganic-organic thin film structures by molecular layer deposition: A review. *Beilstein J. Nanotechnol.* **2014**, *5* (1), 1104–36.
- (51) Liang, X.; Li, J.; Yu, M.; McMurray, C. N.; Falconer, J. L.; Weimer, A. W. Stabilization of Supported Metal Nanoparticles Using an Ultrathin Porous Shell. *ACS Catal.* **2011**, *1* (10), 1162–1165.
- (52) Gould, T. D.; Izar, A.; Weimer, A. W.; Falconer, J. L.; Medlin, J. W. Stabilizing Ni Catalysts by Molecular Layer Deposition for Harsh, Dry Reforming Conditions. *ACS Catal.* **2014**, *4* (8), 2714–2717.
- (53) Goulas, A.; Dokania, A.; Grillo, F.; van Ommen, J. R.; van Limpt, B. Scalable Production of Stabilized Catalysts via Atomic Layer Deposition. *TechConnect Briefs* **2015**, *2*, 120–123.
- (\$4) Yi, H.; Du, H.; Hu, Y.; Yan, H.; Jiang, H.-L.; Lu, J. Precisely Controlled Porous Alumina Overcoating on Pd Catalyst by Atomic Layer Deposition: Enhanced Selectivity and Durability in Hydrogenation of 1,3-Butadiene. ACS Catal. 2015, 5 (\$5), 2735–2739.
- (55) Kennedy, R. M.; Crosby, L. A.; Ding, K.; Canlas, C. P.; Gulec, A.; Marks, L. D.; Elam, J. W.; Marshall, C. L.; Poeppelmeier, K. R.; Stair, P. C. Replication of SMSI via ALD: TiO2 Overcoats Increase Pt-Catalyzed Acrolein Hydrogenation Selectivity. *Catal. Lett.* **2018**, 148 (8), 2223–2232.
- (56) Héroguel, F.; Le Monnier, B. P.; Brown, K. S.; Siu, J. C.; Luterbacher, J. S. Catalyst stabilization by stoichiometrically limited layer-by-layer overcoating in liquid media. *Appl. Catal., B* **2017**, *218*, 643–649.
- (57) Le Monnier, B. P.; Wells, F.; Talebkeikhah, F.; Luterbacher, J. S. Atomic Layer Deposition on Dispersed Materials in Liquid Phase by Stoichiometrically Limited Injections. *Adv. Mater.* **2019**, *31* (52), 1970373.
- (58) Alba-Rubio, A. C.; O'Neill, B. J.; Shi, F.; Akatay, C.; Canlas, C.; Li, T.; Winans, R.; Elam, J. W.; Stach, E. A.; Voyles, P. M.; Dumesic, J. A. Pore Structure and Bifunctional Catalyst Activity of Overlayers Applied by Atomic Layer Deposition on Copper Nanoparticles. *ACS Catal.* **2014**, *4* (5), 1554–1557.
- (59) Li, T.; Karwal, S.; Aoun, B.; Zhao, H.; Ren, Y.; Canlas, C. P.; Elam, J. W.; Winans, R. E. Exploring Pore Formation of Atomic Layer-Deposited Overlayers by in Situ Small- and Wide-Angle X-ray Scattering. *Chem. Mater.* **2016**, *28* (19), 7082–7087.
- (60) Johnson, R. W.; Hultqvist, A.; Bent, S. F. A brief review of atomic layer deposition: from fundamentals to applications. *Mater. Today* **2014**, *17* (5), 236–246.
- (61) Tauster, S. J. Strong Metal-Support Interactions. *Acc. Chem. Res.* **1987**, 20 (11), 389–394.
- (62) Tauster, S. J.; Fung, S. C.; Garten, R. L. Strong Metal-Support Interactions. Group 8 Noble Metals Supported on TiO2. *J. Am. Chem. Soc.* 1978, 100, 170–175.
- (63) Tauster, S. J.; Fung, S. C. Strong Metal-Support Interactions: Occurrence among the Binary Oxides of Groups IIA-VB. *J. Catal.* 1978, 55, 29–35.
- (64) Lunkenbein, T.; Schumann, J.; Behrens, M.; Schlogl, R.; Willinger, M. G. Formation of a ZnO overlayer in industrial Cu/ZnO/Al2O3 catalysts induced by strong metal-support interactions. *Angew. Chem., Int. Ed.* **2015**, *54* (15), 4544–4548.
- (65) Sá, J.; Bernardi, J.; Anderson, J. A. Imaging of low temperature induced SMSI on Pd/TiO2 catalysts. *Catal. Lett.* **2007**, *114* (1–2), 91–95.
- (66) Tang, H.; Su, Y.; Zhang, B.; Lee, A. F.; Isaacs, M. A.; Wilson, K.; Li, L.; Ren, Y.; Huang, J.; Haruta, M.; Qiao, B.; Liu, X.; Jin, C.; Su, D.; Wang, J.; Zhang, T. Classical strong metal-support interactions between gold nanoparticles and titanuium dioxide. *Sci. Adv.* 2017, 3 (10), e1700231.
- (67) Sexton, B. A.; Hughes, A. E.; Foger, K. XPS Investigation of Strong Metal-Support Interactions on Group IIIa-Va Oxides. *J. Catal.* **1982**, 77, 85–93.

- (68) Sanchez, M. G.; Gazquez, J. L. Oxygen Vacancy Model in Strong Metal-Support interaction. *J. Catal.* **1987**, *104*, 120–135.
- (69) Baker, R. T.; Prestridge, E. B.; Garten, R. L. Electron Microscopy of Supported Metal Particles I. Behavior of Pt on Titanium Oxide, Aluminum Oxide, Silicon Oxide, and Carbon. *J. Catal.* 1979, 56 (3), 390–406.
- (70) Baker, R. T.; Prestridge, E. B.; Garten, R. L. Electron Microscopy of Supported Metal Particles II. Further Studies of Pt/TiO2. *J. Catal.* **1979**, *59* (2), 293–302.
- (71) Gao, Y.; Liang, Y.; Chambers, S. A. Thermal stability and the role of oxygen vacancy defects in strong metal support interaction- Pt on Nb-doped TiO2(100). *Surf. Sci.* **1996**, *365*, 638–648.
- (72) Fu, J.; Yue, Q.; Guo, H.; Ma, C.; Wen, Y.; Zhang, H.; Zhang, N.; Zheng, Y.; Zheng, J.; Chen, B.-H. Constructing Pd/CeO2/C To Achieve High Leaching Resistance and Activity for Catalytic Wet Air Oxidation of Aqueous Amide. ACS Catal. 2018, 8 (6), 4980–4985.
- (73) Tang, H.; Wei, J.; Liu, F.; Qiao, B.; Pan, X.; Li, L.; Liu, J.; Wang, J.; Zhang, T. Strong Metal—Support Interactions between Gold Nanoparticles and Nonoxides. *J. Am. Chem. Soc.* **2016**, *138* (1), 56–59.
- (74) Tang, H.; Liu, F.; Wei, J.; Qiao, B.; Zhao, K.; Su, Y.; Jin, C.; Li, L.; Liu, J. J.; Wang, J.; Zhang, T. Ultrastable Hydroxyapatite/ Titanium-Dioxide-Supported Gold Nanocatalyst with Strong Metal-Support Interaction for Carbon Monoxide Oxidation. *Angew. Chem., Int. Ed.* **2016**, *55* (36), 10606–10611.
- (75) Liu, X.; Liu, M.-H.; Luo, Y.-C.; Mou, C.-Y.; Lin, S. D.; Cheng, H.; Chen, J.-M.; Lee, J.-F.; Lin, T.-S. Strong Metal—Support Interactions between Gold Nanoparticles and ZnO Nanorods in CO Oxidation. *J. Am. Chem. Soc.* **2012**, *134* (24), 10251–10258.
- (76) Liu, S.; Xu, W.; Niu, Y.; Zhang, B.; Zheng, L.; Liu, W.; Li, L.; Wang, J. Ultrastable Au nanoparticles on titania through an encapsulation strategy under oxidative atmosphere. *Nat. Commun.* **2019**, *10* (1), 5790.
- (77) Matsubu, J. C.; Zhang, S.; DeRita, L.; Marinkovic, N. S.; Chen, J. G.; Graham, G. W.; Pan, X.; Christopher, P. Adsorbate-mediated strong metal-support interactions in oxide-supported Rh catalysts. *Nat. Chem.* **2017**, *9* (2), 120–127.
- (78) Chandler, B. D. Strong metal-support interactions: An extra layer of complexity. *Nat. Chem.* **2017**, *9* (2), 108–109.
- (79) Zhang, J.; Wang, H.; Wang, L.; Ali, S.; Wang, C.; Wang, L.; Meng, X.; Li, B.; Su, D. S.; Xiao, F. S. Wet-Chemistry Strong Metal-Support Interactions in Titania-Supported Au Catalysts. *J. Am. Chem. Soc.* **2019**, *141* (7), 2975–2983.
- (80) Wang, L.; Zhang, J.; Zhu, Y.; Xu, S.; Wang, C.; Bian, C.; Meng, X.; Xiao, F.-S. Strong Metal—Support Interactions Achieved by Hydroxide-to-Oxide Support Transformation for Preparation of Sinter-Resistant Gold Nanoparticle Catalysts. *ACS Catal.* **2017**, 7 (11), 7461–7465.
- (81) Lee, J.; Burt, S. P.; Carrero, C. A.; Alba-Rubio, A. C.; Ro, I.; O'Neill, B. J.; Kim, H. J.; Jackson, D. H. K.; Kuech, T. F.; Hermans, I.; Dumesic, J. A.; Huber, G. W. Stabilizing cobalt catalysts for aqueous-phase reactions by strong metal-support interaction. *J. Catal.* **2015**, 330, 19–27.
- (82) Wang, Y.-H.; Liu, H.-M.; Xu, B.-Q. Durable Ni/MgO catalysts for CO2 reforming of methane: Activity and metal-support interaction. *J. Mol. Catal. A: Chem.* **2009**, 299 (1–2), 44–52.
- (83) Gonzalez-DelaCruz, V. M.; Holgado, J. P.; Pereniguez, R.; Caballero, A. Morphology changes induced by strong metal—support interaction on a Ni–ceria catalytic system. *J. Catal.* **2008**, 257 (2), 307–314.
- (84) Caballero, A.; Holgado, J. P.; Gonzalez-delaCruz, V. M.; Habas, S. E.; Herranz, T.; Salmeron, M. In situ spectroscopic detection of SMSI effect in a Ni/CeO2 system: hydrogen-induced burial and dig out of metallic nickel. *Chem. Commun.* **2010**, *46* (7), 1097–1099.
- (85) Li, S.; Zhang, C.; Huang, Z.; Wu, G.; Gong, J. A Ni@ZrO2 nanocomposite for ethanol steam reforming: enhanced stability via strong metal-oxide interaction. *Chem. Commun.* **2013**, 49 (39), 4226–4228.

- (86) Nishihata, Y.; Mizuki, J.; Akao, T.; Tanaka, H.; Uenishi, M.; Kimura, M.; Okamoto, T.; Hamada, N. Self-regeneration of a Pdperovskite catalyst for automotive emissions control. *Nature* **2002**, 418 (6894), 164–167.
- (87) Onn, T. M.; Monai, M.; Dai, S.; Fonda, E.; Montini, T.; Pan, X.; Graham, G. W.; Fornasiero, P.; Gorte, R. J. Smart Pd Catalyst with Improved Thermal Stability Supported on High-Surface-Area LaFeO3 Prepared by Atomic Layer Deposition. *J. Am. Chem. Soc.* **2018**, *140* (14), 4841–4848.
- (88) Deng, J.; Cai, M.; Sun, W.; Liao, X.; Chu, W.; Zhao, X. S. Oxidative methane reforming with an intelligent catalyst: sintering-tolerant supported nickel nanoparticles. *ChemSusChem* **2013**, *6* (11), 2061–2065.
- (89) Stöber, W.; Fink, A.; Bohn, E. Controlled growth of monodisperse silica spheres in the micron size range. *J. Colloid Interface Sci.* 1968, 26 (1), 62–69.
- (90) Liu, S. H.; Han, M. Y. Synthesis, Functionalization, and Bioconjugation of Monodisperse, Silica-Coated Gold Nanoparticles: Robust Bioprobes. *Adv. Funct. Mater.* **2005**, *15* (6), 961–967.
- (91) Wang, H.; Zhang, J.-f.; Bai, Y.-x.; Wang, W.-f.; Tan, Y.-s.; Han, Y.-z. NiO@SiO2 core-shell catalyst for low-temperature methanation of syngas in slurry reactor. *J. Fuel Chem. Technol.* **2016**, 44 (5), 548–556.
- (92) Rogach, A. L.; Nagesha, D.; Ostrander, J. W.; Giersig, M.; Kotov, N. A. Raisin Bun"-Type Composite Spheres of Silica and Semiconductor Nanocrystals. *Chem. Mater.* **2000**, *12* (9), 2676–2685.
- (93) Liu, Y. D.; Fang, F. F.; Choi, H. J. Silica nanoparticle decorated polyaniline nanofiber and its electrorheological response. *Soft Matter* **2011**, 7 (6), 2782–2789.
- (94) Zhang, Y.; Cao, M.; Yao, Z.; Wang, Z.; Song, Z.; Ullah, A.; Hao, H.; Liu, H. Effects of silica coating on the microstructures and energy storage properties of BaTiO3 ceramics. *Mater. Res. Bull.* **2015**, *67*, 70–76.
- (95) Tartaj, P.; Serna, C. J. Synthesis of Monodisperse Superparamagnetic Fe/Silica Nanospherical Composites. *J. Am. Chem. Soc.* **2003**, *125*, 15754–15755.
- (96) Lu, Y.; Yin, Y.; Li, Z.-Y.; Xia, Y. Synthesis and Self-Assembly of Au@SiO2 Core-Shell Colloids. *Nano Lett.* **2002**, *2* (7), 785–788.
- (97) Ashik, U. P. M.; Wan Daud, W. M. A. Nanonickel catalyst reinforced with silicate for methane decomposition to produce hydrogen and nanocarbon: synthesis by co-precipitation cum modified Stöber method. *RSC Adv.* **2015**, *5* (58), 46735–46748.
- (98) Ashik, U. P. M.; Daud, W. M. A. W. Probing the differential methane decomposition behaviors of n-Ni/SiO2, n-Fe/SiO2 and n-Co/SiO2 catalysts prepared by co-precipitation cum modified Stöber method. *RSC Adv.* **2015**, *5* (82), *67227*–*67241*.
- (99) Yang, W.; Liu, H.; Li, Y.; Zhang, J.; Wu, H.; He, D. Properties of yolk—shell structured Ni@SiO2 nanocatalyst and its catalytic performance in carbon dioxide reforming of methane to syngas. *Catal. Today* **2016**, 259, 438–445.
- (100) Han, Y.; Wen, B.; Zhu, M. Core-Shell Structured Ni@SiO2 Catalysts Exhibiting Excellent Catalytic Performance for Syngas Methanation Reactions. *Catalysts* **2017**, *7* (1), 21.
- (101) Wang, J.; Zhang, M.; Xu, J.; Zheng, J.; Hayat, T.; Alharbi, N. S. Formation of Fe3O4@C/Ni microtubes for efficient catalysis and protein adsorption. *Dalton Trans.* **2018**, 47 (8), 2791–2798.
- (102) Pang, Y.; Dou, Y.; Zhong, A.; Jiang, W.; Gu, L.; Feng, X.; Ji, W.; Au, C.-T. Nanostructured Ru-Co@SiO2: Highly efficient yet durable for CO2 reforming of methane with a desirable H2/CO ratio. *Appl. Catal., A* **2018**, *SSS*, 27–35.
- (103) Habibi, A. H.; Hayes, R. E.; Semagina, N. Bringing attention to metal (un)availability in encapsulated catalysts. *Catal. Sci. Technol.* **2018**, *8* (3), 798–805.
- (104) Habibi, A. H.; Hayes, R. E.; Semagina, N. Evaluation of hydrothermal stability of encapsulated PdPt@SiO2 catalyst for lean CH4 combustion. *Appl. Catal., A* **2018**, *556*, 129–136.
- (105) Saxena, S.; Singh, R.; Pala, R. G. S.; Sivakumar, S. Sinterresistant gold nanoparticles encapsulated by zeolite nanoshell for oxidation of cyclohexane. *RSC Adv.* **2016**, *6* (10), 8015–8020.

- (106) Chen, J.; Xue, Z.; Feng, S.; Tu, B.; Zhao, D. Synthesis of mesoporous silica hollow nanospheres with multiple gold cores and catalytic activity. *J. Colloid Interface Sci.* **2014**, 429, 62–67.
- (107) Ashik, U. P. M.; Wan Daud, W. M. A.; Abbas, H. F. Methane decomposition kinetics and reaction rate over Ni/SiO2 nanocatalyst produced through co-precipitation cum modified Stöber method. *Int. J. Hydrogen Energy* **2017**, *42* (2), 938–952.
- (108) Cargnello, M.; Fornasiero, P.; Gorte, R. J. Opportunities for Tailoring Catalytic Properties Through Metal-Support Interactions. *Catal. Lett.* **2012**, *142* (9), 1043–1048.
- (109) Li, Y.; Lu, G.; Ma, J. Highly active and stable nano NiO-MgO catalyst encapsulated by silica with a core-shell structure for CO2 methanation. *RSC Adv.* **2014**, *4* (34), 17420-17428.
- (110) Ai, Y.; Hu, Z.; Shao, Z.; Qi, L.; Liu, L.; Zhou, J.; Sun, H.; Liang, Q. Egg-like magnetically immobilized nanospheres: A long-lived catalyst model for the hydrogen transfer reaction in a continuous-flow reactor. *Nano Res.* **2018**, *11* (1), 287–299.
- (111) Salgueiriño-Maceira, V.; Correa-Duarte, M. A. Cobalt and silica based core—shell structured nanospheres. *J. Mater. Chem.* **2006**, 16 (36), 3593—3597.
- (112) Kobayashi, Y.; Horie, M.; Konno, M.; Rodriguez-Gonzalez, B.; Liz-Marzan, L. M. Preparation and Properties of Silica-Coated Cobalt Nanoparticles. *J. Phys. Chem. B* **2003**, *107*, 7420–7425.
- (113) Fu, W.; Yang, H.; Hari-Bala; Liu, S.; Li, M.; Zou, G. Preparation and characteristics of core–shell structure cobalt/silica nanoparticles. *Mater. Chem. Phys.* **2006**, *100* (2–3), 246–250.
- (114) Batail, N.; Clémençon, I.; Legens, C.; Chaumonnot, A.; Uzio, D. Controlled Synthesis and High Oxidation Stability of Cobalt Nanoparticles Encapsulated in Mesoporous Silica using a Modified Stöber Approach and a Pseudomorphic Transformation. *Eur. J. Inorg. Chem.* **2013**, 2013 (8), 1258–1264.
- (115) Arnal, P. M.; Comotti, M.; Schüth, F. High-Temperature-Stable Catalysts by Hollow Sphere Encapsulation. *Angew. Chem., Int. Ed.* **2006**, 45 (48), 8224–8227.
- (116) Fang, J.; Zhang, Y.; Zhou, Y.; Zhao, S.; Zhang, C.; Yang, C.; Chen, W.; Huang, M.; Gao, Y. Synthesis of novel ultrasmall Au-loaded magnetic SiO2/carbon yolk-shell ellipsoids as highly reactive and recoverable nanocatalysts. *Carbon* **2017**, *121*, 602–611.
- (117) Yang, Y.; Yang, F.; Zeng, D.; Huang, Z.; Zhang, J.; Hao, S.; Kong, X.; Zhang, Z.; Liu, B. Surfactant-free synthesis of hollow mesoporous carbon spheres and their encapsulated Au derivatives using biopolymeric chitosan. *J. Colloid Interface Sci.* **2018**, 531, 291–299.
- (118) Li, K.-T.; Hsu, M.-H.; Wang, I. Palladium core—porous silica shell-nanoparticles for catalyzing the hydrogenation of 4-carbox-ybenzaldehyde. *Catal. Commun.* **2008**, *9* (13), 2257–2260.
- (119) Joo, S. H.; Park, J. Y.; Tsung, C. K.; Yamada, Y.; Yang, P.; Somorjai, G. A. Thermally stable Pt/mesoporous silica core-shell nanocatalysts for high-temperature reactions. *Nat. Mater.* **2009**, *8* (2), 126–131.
- (120) Shang, L.; Bian, T.; Zhang, B.; Zhang, D.; Wu, L. Z.; Tung, C. H.; Yin, Y.; Zhang, T. Graphene-supported ultrafine metal nanoparticles encapsulated by mesoporous silica: robust catalysts for oxidation and reduction reactions. *Angew. Chem., Int. Ed.* **2014**, *53* (1), 250–254.
- (121) Styskalik, A.; Skoda, D.; Barnes, C.; Pinkas, J. The Power of Non-Hydrolytic Sol-Gel Chemistry: A Review. *Catalysts* **2017**, *7* (6), 168.
- (122) Vioux, A. Nonhydrolytic sol-gel routes to oxides. *Chem. Mater.* **1997**, *9* (11), 2292–2299.
- (123) Debecker, D.; Mutin, P. Non-hydrolytic sol-gel routes to heterogeneous catalysts. *Chem. Soc. Rev.* **2012**, *41* (9), 3624–3650.
- (124) Debecker, D.; Bouchmella, K.; Stoyanova, M.; Rodemerck, U.; Gaigneaux, E.; Hubert Mutin, P. A non-hydrolytic sol-gel route to highly active MoO<sub>3</sub>-SiO<sub>2</sub>-Al<sub>2</sub>O<sub>3</sub> metathesis catalysts. *Catal. Sci. Technol.* **2012**, *2* (6), 1157–1164.
- (125) Debecker, D.; Hulea, V.; Mutin, P. Mesoporous mixed oxide catalysts via non-hydrolytic sol-gel: A review. *Appl. Catal., A* **2013**, 451, 192–206.

- (126) Skoda, D.; Styskalik, A.; Moravec, Z.; Bezdicka, P.; Bursik, J.; Mutin, P.; Pinkas, J. Mesoporous SnO2-SiO2 and Sn-silica-carbon nanocomposites by novel non-hydrolytic templated sol-gel synthesis. *RSC Adv.* **2016**, *6* (73), 68739–68747.
- (127) Skoda, D.; Styskalik, A.; Moravec, Z.; Bezdicka, P.; Barnes, C.; Pinkas, J. Mesoporous titanosilicates by templated non-hydrolytic solgel reactions. *J. Sol-Gel Sci. Technol.* **2015**, 74 (3), 810–822.
- (128) Sboui, M.; Bouattour, S.; Gruttadauria, M.; Liotta, L.; La Parola, V.; Boufi, S. Hybrid paper-TiO2 coupled with a Cu2O heterojunction: an efficient photocatalyst under sun-light irradiation. *RSC Adv.* **2016**, *6* (90), 86918–86929.
- (129) Moggi, P.; Devillers, M.; Ruiz, P.; Predieri, G.; Cauzzi, D.; Morselli, S.; Ligabue, O. Oxidative dehydrogenation of propane on pure and silica-dispersed multimetallic oxides based on vanadium and niobium prepared via hydrolytic and non-hydrolytic sol-gel methods. *Catal. Today* **2003**, *81* (2), 77–85.
- (130) Petitto, C.; Mutin, H.; Delahay, G. Hydrothermal activation of silver supported alumina catalysts prepared by sol-gel method: Application to the selective catalytic reduction (SCR) of NOx by n-decane. *Appl. Catal., B* **2013**, *134*, 258–264.
- (131) Nguyen, P.; Salim, C.; Kurniawan, W.; Hinode, H. A non-hydrolytic sol-gel synthesis of reduced graphene oxide/TiO2 microsphere photocatalysts. *Catal. Today* **2014**, 230, 166–173.
- (132) de Lima, O.; Papacidero, A.; Rocha, L.; Sacco, H.; Nassar, E.; Ciuffi, K.; Bueno, L.; Messaddeq, Y.; Ribeiro, S. Sol-gel entrapped cobalt complex. *Mater. Charact.* **2003**, *50* (2–3), 101–108.
- (133) Mac Leod, T.; Guedes, D.; Lelo, M.; Rocha, R.; Caetano, B.; Ciuffi, K.; Assis, M. Catalytic activity of Jacobsen catalyst encapsulated in an alumina matrix by the sol-gel process. *J. Mol. Catal. A: Chem.* **2006**, 259 (1–2), 319–327.
- (134) Bouchmella, K.; Hubert Mutin, P.; Stoyanova, M.; Poleunis, C.; Eloy, P.; Rodemerck, U.; Gaigneaux, E.; Debecker, D. Olefin metathesis with mesoporous rhenium-silicium-aluminum mixed oxides obtained via a one-step non-hydrolytic sol-gel route. *J. Catal.* **2013**, *301*, 233–241.
- (135) Héroguel, F.; Silvioli, L.; Du, Y.; Luterbacher, J. Controlled deposition of titanium oxide overcoats by non-hydrolytic sol gel for improved catalyst selectivity and stability. *J. Catal.* **2018**, 358, 50–61.
- (136) Ykrelef, A.; Nadji, L.; Issaadi, R.; Agouram, S.; Rodriguez-Castellon, E.; Solsona, B.; Lopez Nieto, J. M. Mixed oxide Ti-Si-O prepared by non-hydrolytic Xerogel method as a diluter of nickel oxide for the oxidative dehydrogenation of ethane. *Catal. Today* **2018**, 299, 93–101.
- (137) Debecker, D.; Bouchmella, K.; Delaigle, R.; Eloy, P.; Poleunis, C.; Bertrand, P.; Gaigneaux, E.; Mutin, P. One-step non-hydrolytic sol-gel preparation of efficient V2O5-TiO2 catalysts for VOC total oxidation. *Appl. Catal., B* **2010**, *94* (1–2), 38–45.
- (138) Debecker, D.; Delaigle, R.; Bouchmella, K.; Eloy, P.; Gaigneaux, E.; Mutin, P. Total oxidation of benzene and chlorobenzene with MoO3- and WO3-promoted V2O5/TiO2 catalysts prepared by a nonhydrolytic sol-gel route. *Catal. Today* **2010**, *157* (1–4), 125–130.
- (139) Nadji, L.; Masso, A.; Delgado, D.; Issaadi, R.; Rodriguez-Aguado, E.; Rodriguez-Castellon, E.; Nieto, J. Gas phase dehydration of glycerol to acrolein over WO3-based catalysts prepared by non-hydrolytic sol-gel synthesis. *RSC Adv.* **2018**, *8* (24), 13344–13352.
- (140) Ricci, G.; Rocha, Z.; Nakagaki, S.; Castro, K.; Crotti, A.; Calefi, P.; Nassar, E.; Ciuffi, K. Iron-alumina materials prepared by the non-hydrolytic sol-gel route: Synthesis, characterization and application in hydrocarbons oxidation using hydrogen peroxide as oxidant. *Appl. Catal., A* **2010**, 389 (1–2), 147–154.
- (141) Secordel, X.; Yoboue, A.; Cristol, S.; Lancelot, C.; Capron, M.; Paul, J.; Berrier, E. Supported oxorhenate catalysts prepared by thermal spreading of metal Re0 for methanol conversion to methylal. *J. Solid State Chem.* **2011**, *184* (10), 2806–2811.
- (142) Bouchmella, K.; Stoyanova, M.; Rodemerck, U.; Debecker, D.; Hubert Mutin, P. Avoiding rhenium loss in non-hydrolytic synthesis of highly active Re-Si-Al olefin metathesis catalysts. *Catal. Commun.* **2015**, *58*, 183–186.

- (143) Smeets, V.; Ben Mustapha, L.; Schnee, J.; Gaigneaux, E.; Debecker, D. Mesoporous SiO2-TiO2 epoxidation catalysts: Tuning surface polarity to improve performance in the presence of water. *Mol. Catal.* **2018**, *452*, 123–128.
- (144) Oakton, E.; Siddiqi, G.; Fedorov, A.; Coperet, C. Tungsten oxide by non-hydrolytic sol-gel: effect of molecular precursor on morphology, phase and photocatalytic performance. *New J. Chem.* **2016**, *40* (1), 217–222.
- (145) Ullmann, M.; Bernardes, A.; dos Santos, J. Silica-supported metallocene catalyst poisoning: The effect of surface modification on the efficiency of the catalytic system. *Colloids Surf., A* **2019**, *565*, 36–46
- (146) Pham, H. N.; Anderson, A. E.; Johnson, R. L.; Schmidt-Rohr, K.; Datye, A. K. Improved hydrothermal stability of mesoporous oxides for reactions in the aqueous phase. *Angew. Chem., Int. Ed.* **2012**, *51* (52), 13163–13167.
- (147) Lin, W.; Cheng, H.; Ming, J.; Yu, Y.; Zhao, F. Deactivation of Ni/TiO2 catalyst in the hydrogenation of nitrobenzene in water and improvement in its stability by coating a layer of hydrophobic carbon. *J. Catal.* **2012**, 291, 149–154.
- (148) Jenkins, A. H.; Musgrave, C. B.; Medlin, J. W. Enhancing Au/TiO2 Catalyst Thermostability and Coking Resistance with Alkyl Phosphonic-Acid Self-Assembled Monolayers. *ACS Appl. Mater. Interfaces* **2019**, *11* (44), 41289–41296.
- (149) van den Berg, R.; Parmentier, T. E.; Elkjær, C. F.; Gommes, C. J.; Sehested, J.; Helveg, S.; de Jongh, P. E.; de Jong, K. P. Support Functionalization To Retard Ostwald Ripening in Copper Methanol Synthesis Catalysts. *ACS Catal.* **2015**, *5* (7), 4439–4448.
- (150) Gawande, M. B.; Goswami, A.; Asefa, T.; Guo, H.; Biradar, A. V.; Peng, D.-L.; Zboril, R.; Varma, R. S. Core—shell nanoparticles: synthesis and applications in catalysis and electrocatalysis. *Chem. Soc. Rev.* **2015**, *44* (21), 7540–7590.
- (151) Bakhmutsky, K.; Wieder, N. L.; Cargnello, M.; Galloway, B.; Fornasiero, P.; Gorte, R. J. A versatile route to core-shell catalysts: synthesis of dispersible M@oxide (M = Pd, Pt; oxide = TiO2, ZrO2) nanostructures by self-assembly. *ChemSusChem* **2012**, 5 (1), 140–148.
- (152) Arroyo-Ramírez, L.; Chen, C.; Cargnello, M.; Murray, C. B.; Gorte, R. J. A comparison of hierarchical Pt@CeO2/Si-Al2O3 and Pd@CeO2/Si-Al2O3. *Catal. Today* **2015**, 253, 137–141.
- (153) Cargnello, M.; Montini, T.; Polizzi, S.; Wieder, N. L.; Gorte, R. J.; Graziani, M.; Fornasiero, P. Novel embedded Pd@CeO2 catalysts: a way to active and stable catalysts. *Dalton Trans.* **2010**, 39 (8), 2122–2127.
- (154) Cargnello, M.; Wieder, N. L.; Montini, T.; Gorte, R. J.; Fornasiero, P. Synthesis of Dispersible Pd@CeO2 Core—Shell Nanostructures by Self-Assembly. *J. Am. Chem. Soc.* **2010**, *132* (4), 1402–1409.
- (155) Cargnello, M.; Jaén, J. D.; Garrido, J. C. H.; Bakhmutsky, K.; Montini, T.; Gámez, J. J. C.; Gorte, R. J.; Fornasiero, P. Exceptional Activity for Methane Combustion over Modular Pd@CeO2 Subunits on Functionalized Al2O3. *Science* 2012, 337, 713–717.
- (156) Adijanto, L.; Bennett, D. A.; Chen, C.; Yu, A. S.; Cargnello, M.; Fornasiero, P.; Gorte, R. J.; Vohs, J. M. Exceptional thermal stability of Pd@CeO2 core-shell catalyst nanostructures grafted onto an oxide surface. *Nano Lett.* **2013**, *13* (5), 2252–2257.
- (157) Zhang, N.; Xu, Y.-J. Aggregation- and Leaching-Resistant, Reusable, and Multifunctional Pd@CeO2 as a Robust Nanocatalyst Achieved by a Hollow Core—Shell Strategy. *Chem. Mater.* **2013**, *25* (9), 1979—1988.
- (158) Forman, A. J.; Park, J.-N.; Tang, W.; Hu, Y.-S.; Stucky, G. D.; McFarland, E. W. Silica-Encapsulated Pd Nanoparticles as a Regenerable and Sintering-Resistant Catalyst. *ChemCatChem* **2010**, 2 (10), 1318–1324.
- (159) Hayashi, H.; Chen, L. Z.; Tago, T.; Kishida, M.; Wakabayashi, K. Catalytic properties of Fe/SiO2 catalysts prepared using microemulsion for CO hydrogenation. *Appl. Catal., A* **2002**, *231* (1–2), 81–89.

- (160) Park, J. N.; Forman, A. J.; Tang, W.; Cheng, J.; Hu, Y. S.; Lin, H.; McFarland, E. W. Highly active and sinter-resistant Pd-nanoparticle catalysts encapsulated in silica. *Small* **2008**, *4* (10), 1694–1697.
- (161) Ying, J.; Peng, H.; Xu, X.; Wang, R.; Yu, F.; Sun, Q.; Liu, W.; Gao, Z.; Wang, X. Thermally stable ultra-small Pd nanoparticles encapsulated by silica: elucidating the factors determining the inherent activity of noble metal catalysts. *Catal. Sci. Technol.* **2016**, 6 (14), 5405–5414.
- (162) Zhang, T.; Li, B.; Zhang, X.; Qiu, J.; Han, W.; Yeung, K. L. Pd nanoparticles immobilized in a microporous/mesoporous composite ZIF-8/MSS: A multifunctional catalyst for the hydrogenation of alkenes. *Microporous Mesoporous Mater.* **2014**, *197*, 324–330.
- (163) Yu, K.; Wu, Z.; Zhao, Q.; Li, B.; Xie, Y. High-Temperature-Stable Au@SnO2 Core/Shell Supported Catalyst for CO Oxidation. *J. Phys. Chem. C* **2008**, *112* (7), 2244–2247.
- (164) Chen, C.; Shi, M.; Cargnello, M.; Fornasiero, P.; Murray, C. B.; Gorte, R. J. Au@TiO2 Core—Shell Nanostructures with High Thermal Stability. *Catal. Lett.* **2014**, *144* (11), 1939–1945.
- (165) Cargnello, M.; Gentilini, C.; Montini, T.; Fonda, E.; Mehraeen, S.; Chi, M.; Herrera-Collado, M.; Browning, N. D.; Polizzi, S.; Pasquato, L.; Fornasiero, P. Active and Stable Embedded Au@CeO2 Catalysts for Preferential Oxidation of CO. *Chem. Mater.* 2010, 22 (14), 4335–4345.
- (166) Zhu, J.; Konya, Z.; Puntes, V. F.; Kiricsi, I.; Miao, C. X.; Ager, J. W.; Alivisatos, A. P.; Somorjai, G. A. Encapsulation of Metal (Au, Ag, Pt) Nanoparticles into the Mesoporous SBA-15 Structure. *Langmuir* **2003**, *19* (10), 4396–4401.
- (167) Yang, H.; Lu, Q.; Gao, F.; Shi, Q.; Yan, Y.; Zhang, F.; Xie, S.; Tu, B.; Zhao, D. One-Step Synthesis of Highly Ordered Mesoporous Silica Monoliths with Metal Oxide Nanocrystals in their Channels. *Adv. Funct. Mater.* **2005**, *15* (8), 1377–1384.
- (168) Sreevardhan Reddy, S.; David Raju, B.; Padmasri, A. H.; Sai Prakash, P. K.; Rama Rao, K. S. Novel and efficient cobalt encapsulated SBA-15 catalysts for the selective oxidation of cyclohexane. *Catal. Today* **2009**, *141* (1–2), 61–65.
- (169) Martínez, F.; Calleja, G.; Melero, J. A.; Molina, R. Heterogeneous photo-Fenton degradation of phenolic aqueous solutions over iron-containing SBA-15 catalyst. *Appl. Catal., B* **2005**, 60 (3–4), 181–190.